Inorganic Chemistry

ARTICLE

pubs.acs.org/IC

# Relationship between the Thermally Induced Reorientations of Aromatic Solvate Molecules in Cu(hfac)$_2$−Nitroxide Breathing Crystals and the Character of the Magnetic Anomaly

Galina V. Romanenko, Ksenia Yu. Maryunina, Artem S. Bogomyakov, Renad Z. Sagdeev, and Victor I. Ovcharenko*

International Tomography Center, Siberian Branch of the Russian Academy of Sciences, 3A Institutskaya Street, 630090 Novosibirsk, Russia

Supporting Information

**ABSTRACT:** A new group of "breathing" crystals has been synthesized. These are aromatic solvates of the copper(II) hexafluoroacetylacetonate complex with spin-labeled pyrazole Cu(hfac)$_2$L·0.5Solv, where L is 2-(1-butyl-1*H*-pyrazol-4-yl)-4,4,5,5-tetramethyl-4,5-dihydro-1*H*-imidazole-3-oxide-1-oxyl and Solv is benzene, toluene, ethylbenzene, propylbenzene, butylbenzene, styrene, *o*-xylene, *m*-xylene, *p*-xylene, 1,4-bis(trifluoromethyl)benzene, 1-methyl-4-ethylbenzene, 1-methyl-4-vinylbenzene, 1,4-diethylbenzene, 1,2,3-trimethylbenzene, or 1,2,4-trimethylbenzene. The main feature of Cu(hfac)$_2$L·0.5Solv single crystals is their remarkable mechanical stability and ability to undergo thermally induced structural rearrangements accompanied by spin-crossover-like phenomena. The structures of Cu(hfac)$_2$L·0.5Solv solvates are similar and based on mutually parallel {Cu(hfac)$_2$L}$_\infty$ heterospin chains with a "head-to-head" motif. The localization of voids with guest molecules being the same in all crystals, the temperature dependence of the effective magnetic moment ($\mu_{eff}$) for Cu(hfac)$_2$L·0.5Solv is determined by the structure of the guest molecules, along which the polymer chains are "gliding" when the temperature changes. When the temperature decreased from 300 to 100−50 K, $\mu_{eff}$ decreased, abruptly or gradually, from 2.7−2.4 to ∼1.8 $\beta$ for the majority of Cu(hfac)$_2$L·0.5Solv except the solvates with benzene, toluene, and 1,4-bis(trifluoromethyl)benzene. When Cu(hfac)$_2$L·0.5C$_6$H$_6$ and Cu(hfac)$_2$L·0.5CH$_3$−C$_6$H$_5$ were cooled to 50 K, $\mu_{eff}$ decreased to ∼2.1−2.2 $\beta$. When Cu(hfac)$_2$L·0.5(1,4-(CF$_3$)$_2$−C$_6$H$_4$) was cooled to 50 K, $\mu_{eff}$ initially decreased from ∼2.7 to 1.9 $\beta$ and then abruptly increased to ∼2.4 $\beta$. A single-crystal X-ray diffraction analysis of each solvate within a temperature range wider than the range of magnetic anomaly temperatures revealed a complex interrelated dynamics of the aromatic solvent guest molecules and heterospin chains. The dynamics largely depended on the orientation of the solvent guest molecules relative to the polymer chains. An analysis of the thermally induced phase transformations revealed a relationship between the structural rearrangement of Cu(hfac)$_2$L·0.5Solv and the form of the magnetic anomaly on the $\mu_{eff}(T)$ curve and between the structural rearrangement of the solvate and the temperature of the magnetic effect.

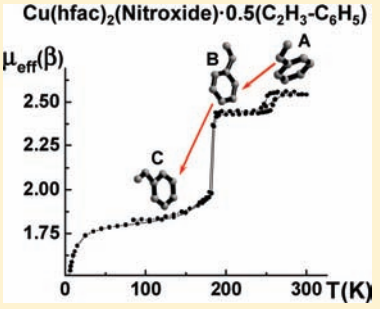


## INTRODUCTION

The heterospin crystals of Cu(II) hexafluoroacetylacetonate complexes with nitroxides are convenient objects for detailed studies of structural rearrangements that cause magnetic anomalies.[1−29] The thermally induced structural rearrangement of the copper−nitroxide exchange cluster provokes magnetic anomalies in the $\mu_{eff}(T)$ dependence which are similar to the classical spin transitions.[30−45] These anomalies, however, are caused by significant changes in the energy of exchange coupling between the odd electrons of paramagnetic centers as opposed to the classical spin transitions.[1−20,22] For stereochemically nonrigid copper complexes with pyrazolyl-substituted derivatives of nitronyl nitroxides, the single crystals often retain their X-ray quality after the transition point, which is an important peculiarity of these compounds.[7,10,13,29] Due to this, one can trace the structure dynamics before and after the phase transition in these "breathing"[9−20] crystals. Previously, it was shown that varying an alkyl substituent in the pyrazole fragment of the paramagnetic ligand considerably affected the structure of the solid[7−10,16,20,29] and hence the magnetic properties of the compounds. It was also reported that modification of coordination units by forming mixed-metal solid solutions was an effective tool for changing the magnetic properties of compounds.[10,12] The temperature of the magnetic anomaly can also be varied within wide limits by forming solid solutions containing different paramagnetic ligands.[10,29] It was found that doping of crystals with definite aliphatic solvent molecules could be used as an efficient method of control over the magnetic anomaly temperature ($T_a$). The "mild" modification of $T_a$ requires a much smaller structural step than the typical change of one −CH$_2$− fragment in a homologous series in organic chemistry.[13,29] Since the solvent guest molecules have only van der Waals interactions with heterospin polymer chains, it was concluded that the interchain interactions were significant

**Received:** March 4, 2011
**Published:** June 15, 2011

and the effect was highly cooperative.[10,13,28,29] It was found that the temperature dynamics of the spin state in exchange clusters showed itself in the EPR spectra of breathing crystals in some specific way, which allowed valuable detailed information about the interactions of paramagnetic centers.[14−21] Studies of the relationship between the structural dynamics and the changes in the magnetic properties also afforded unique information for quantum-chemical analysis of the electronic structure of exchange channels[13,23−25] and development of theoretical approaches to analysis and description of spin transitions in heterospin exchange clusters.[26−28] Recently, another valuable property of these compounds was discovered: they were found to change their spin state when exposed to photoradiation (LIESST effect).[20,21] A radiospectroscopic study of breathing crystals revealed a striking example of noncoincidence between the spatial direction of the polymer chain and the direction of the chain of magnetic interactions.[46]

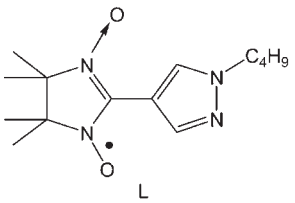


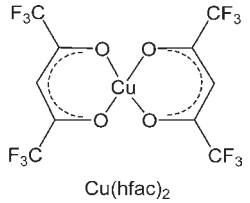


We studied the structural−magnetic correlations inherent in a new group of breathing crystals—the aromatic solvates of the copper(II) hexafluoroacetylacetonate complex with spin-labeled pyrazole $Cu(hfac)_2L\cdot 0.5Solv$, where L is 2-(1-butyl-1*H*-pyrazol-4-yl)-4,4,5,5-tetramethyl-4,5-dihydro-1*H*-imidazole-3-oxide-1-oxyl and Solv is benzene, toluene, ethylbenzene, propylbenzene, butylbenzene, styrene, *o*-xylene, *m*-xylene, *p*-xylene, 1,4-bis(trifluoromethyl)benzene, 1-methyl-4-ethylbenzene, 1-methyl-4-vinylbenzene, 1,4-diethylbenzene, 1,2,3-trimethylbenzene, and 1,2,4-trimethylbenzene. The influence of solvate guest molecules on the character of the magnetic effect was not known from the start; therefore, solvents were chosen that enabled us to trace the transition from simple to complex molecules. Since the benzene ring is a rigid fragment that does not change with temperature, the aromatic derivatives with alkyl substituents were chosen that enabled us to trace the effect of the number of methylene units in the alkyl substituent, the number or mutual arrangement of substituents, and the transition to a substituent with a multiple bond on the characteristics of the magnetic anomaly on the plot of $\mu_{eff}(T)$, namely, the temperature, amplitude, and abruptness. Studies of the relationship between the thermally induced structural rearrangement of $Cu(hfac)_2L\cdot 0.5Solv$ and the character of the magnetic anomaly revealed that the rearrangement of heterospin chains was extremely sensitive to the structure of the solvent guest molecule. It was also found that the thermally induced structure evolution of heterospin chains themselves admitted only definite orientations of aromatic solvent molecules. The temperature dependence of the magnetic moment of breathing crystals can thus serve as an indicator of their supramolecular organization, namely, the existence of definite voids between the chains and the corresponding arrangement of solvent molecules in them.

## EXPERIMENTAL SECTION

**Materials and Physical Techniques.** All solvents were commercially available (Aldrich) and used as received. Nitronyl nitroxide 2-(1-butyl-1*H*-pyrazol-4-yl)-4,4,5,5-tetramethyl-4,5-dihydro-1*H*-imidazole-3-oxide-1-oxyl (L) was prepared as described previously.[47] The $Cu(hfac)_2L\cdot 0.5Solv$ solvates, where Solv is ethylbenzene ($C_2H_5-C_6H_5$), propylbenzene ($C_3H_7-C_6H_5$), butylbenzene ($C_4H_9-C_6H_5$), styrene ($C_2H_3-C_6H_5$), *m*-xylene (1,3-$(CH_3)_2-C_6H_4$), *p*-xylene (1,4-$(CH_3)_2-C_6H_4$), 1,4-bis(trifluoromethyl)benzene (1,4-$(CF_3)_2-C_6H_4$), 1-methyl-4-ethylbenzene (1-$CH_3$-4-$C_2H_5-C_6H_4$), 1-methyl-4-vinylbenzene (1-$CH_3$-4-$C_2H_3-C_6H_4$), 1,4-diethylbenzene (1,4-$(C_2H_5)_2-C_6H_4$), 1,2,3-trimethylbenzene (1,2,3-$(CH_3)_3-C_6H_3$), and 1,2,4-trimethylbenzene (1,2,4-$(CH_3)_3-C_6H_3$), were prepared using the procedure described below for $Cu(hfac)_2L\cdot 0.5C_3H_7-C_6H_5$. The $Cu(hfac)_2L\cdot 0.5Solv$ solvates, where Solv is benzene ($C_6H_6$), toluene ($CH_3-C_6H_5$), or *o*-xylene (1,2-$(CH_3)_2-C_6H_4$), were prepared as described previously.[16] Special care was taken to avoid solvent losses during the experiments. The same freshly prepared crystal batches were used for the X-ray diffraction experiment and measurements of $\mu_{eff}(T)$. All measurements were carried out on an MPMS*XL* SQUID magnetometer (Quantum Design) in the temperature range 2−300 K in a magnetic field of up to 5 kOe. The molar magnetic susceptibility was calculated using diamagnetic corrections for the complexes. The effective magnetic moment was calculated as $\mu_{eff} = (8\chi T)^{1/2}$. The experimental temperature dependences of $\mu_{eff}$ were calculated for the $\{Cu(hfac)_2L\cdot 0.5Solv\}$ unit for all solids. This means that the resulting $\mu_{eff}$ contained the contributions from one-half of all >N−$^{\bullet}$O−$Cu^{II}$−O$^{\bullet}$−N< heterospin clusters belonging to the $CuO_6$ units and from one-half of all isolated Cu(II) ions in the $CuN_2O_4$ coordination units. The magnetic data have good reproducibility for different batches of particular complexes. Measurements of $\mu_{eff}(T)$ were performed at decreasing and increasing temperature for the following complexes exhibiting abrupt magnetic and/or structural phase transitions: $Cu(hfac)_2L\cdot 0.5C_2H_5-C_6H_5$, $Cu(hfac)_2L\cdot 0.5C_2H_3-C_6H_5$, $Cu(hfac)_2L\cdot 0.5C_4H_9-C_6H_5$, $Cu(hfac)_2L\cdot 0.5$(1,4-$(CH_3)_2-C_6H_4$), and $Cu(hfac)_2L\cdot 0.5$(1,4-$(CF_3)_2-C_6H_4$). Hysteresis phenomena were revealed for $Cu(hfac)_2L\cdot 0.5C_2H_3-C_6H_5$ and $Cu(hfac)_2L\cdot 0.5$(1,4-$(CF_3)_2-C_6H_4$).

**Synthesis of Complexes: $Cu(hfac)_2L\cdot 0.5C_3H_7-C_6H_5$.** A mixture of $Cu(hfac)_2$ (0.048 g, 0.10 mmol) and L (0.028 g, 0.10 mmol) was dissolved in propylbenzene (1 mL) placed in a ca. 5 mL glass bottle while quickly heating it from room temperature to 70−75 °C for 2 or 3 min. The heating was then stopped, and the resulting dark brown solution was allowed to spontaneously cool to room temperature. It was kept in an open flask at 5 °C for 1 or 2 days. The resulting dark violet crystals were filtered off, washed with cold heptane, and dried in air. The complex, as well as all other compounds mentioned below, is readily soluble in the majority of organic solvents: Yield 0.065 g, 78%. Anal. Calcd for $C_{28,5}H_{31}N_4O_6F_{12}Cu$: C, 41.9; H, 3.8; N, 6.9; F, 27.9. Found: C, 41.9; H, 3.8; N, 6.8; F, 27.8. $Cu(hfac)_2L\cdot 0.5C_2H_5-C_6H_5$, $Cu(hfac)_2L\cdot 0.5C_2H_3-C_6H_5$, $Cu(hfac)_2L\cdot 0.5C_4H_9-C_6H_5$, $Cu(hfac)_2L\cdot 0.5$(1,3-$(CH_3)_2-C_6H_4$), $Cu(hfac)_2L\cdot 0.5$(1,4-$(CH_3)_2-C_6H_4$), $Cu(hfac)_2L\cdot 0.5$(1,4-$(CF_3)_2-C_6H_4$), $Cu(hfac)_2L\cdot 0.5$(1-$CH_3$-4-$C_2H_5-C_6H_4$), $Cu(hfac)_2L\cdot 0.5$(1-$CH_3$-4-$C_2H_3-C_6H_4$), $Cu(hfac)_2L\cdot 0.5$(1,4-$(C_2H_5)_2-C_6H_4$), $Cu(hfac)_2L\cdot 0.5$(1,2,3-$(CH_3)_3-C_6H_3$), and $Cu(hfac)_2L\cdot 0.5$(1,2,4-$(CH_3)_3-C_6H_3$) were prepared by a similar procedure using ethylbenzene, styrene, butylbenzene, *m*-xylene, *p*-xylene, 1,4-bis(trifluoromethyl)benzene, 1-methyl-4-ethylbenzene, 1-methyl-4-vinylbenzene, 1,4-diethylbenzene, 1,2,3-trimethylbenzene, and 1,2,4-trimethylbenzene, respectively, as a solvent. $Cu(hfac)_2L\cdot 0.5C_2H_5-C_6H_5$: Yield 0.050 g, 61%. Anal. Calcd for $C_{28}H_{30}N_4O_6F_{12}Cu$: C, 41.5; H, 3.7; N, 6.9; F, 28.1. Found: C, 41.6; H, 3.6; N, 7.0; F, 28.2. $Cu(hfac)_2L\cdot 0.5C_2H_3-C_6H_5$: Yield 0.030 g, 37%. Anal. Calcd for $C_{28}H_{29}N_4O_6F_{12}Cu$: C, 41.6; H, 3.6; N, 6.9; F, 28.2. Found: C, 41.6; H, 3.7; N, 7.0; F, 28.3. $Cu(hfac)_2L\cdot 0.5C_4H_9-C_6H_5$: Yield 0.065 g, 85%. Anal. Calcd for $C_{29}H_{32}N_4O_6F_{12}Cu$: C, 42.3; H, 3.9; N, 6.8; F, 27.7. Found: C, 42.6; H, 4.2; N, 7.3; F, 28.2. $Cu(hfac)_2L\cdot 0.5$(1,3-$(CH_3)_2-C_6H_4$): Yield 0.050 g, 62%. Anal. Calcd for $C_{28}H_{30}N_4O_6F_{12}Cu$: C, 41.5; H, 3.7; N,

**Table 1. Magnetic Anomaly Temperatures ($T_a$, K), X-ray Experiment Temperatures (T, K), Type of Orientation of the Solvate Molecule, Temperature Dynamics of the Selected Distances ($d$, Å) for Cu(hfac)$_2$L·0.5Solv, Volume of the Interchain Cavity ($V_{cav}$, Å$^3$), and Experimental Densities ($D_{calcd}$, g/cm$^3$)**

| Solv in Cu(hfac)$_2$L·0.5Solv | $T_a$ | $T$ | orientation type of solv | $d$(Cu−O$_{NO}$) | $d$(Cu−O$_{hfac}$) | $d$(Cu−O$_{hfac}$) | $d$(Cu−N) | $d$(O$_{NO}$···O$_{NO}$) | $V_{cav}$ | $D_{calcd}$ |
|---|---|---|---|---|---|---|---|---|---|---|
| $C_2H_5-C_6H_5$ | 205 | 295 | A | 2.332(2) | 1.974(2) | 1.963(2) | 2.497(3) | 4.186 | 268 | 1.501 |
| | | 240 | B | 2.322(2) | 1.979(2) | 2.007(1) | 2.359(3) | 3.361 | 255 | 1.483 |
| | | 215 | B | 2.303(3) | 1.967(3) | 1.994(3) | 2.332(3) | 3.317 | 241 | 1.522 |
| | | 180 | C | 2.018(2) | 2.207(2) | 2.009(2) | 2.461(2) | 3.437 | 240 | 1.601 |
| | | 120 | C | 1.997(2) | 2.264(2) | 1.996(2) | 2.454(6) | 3.398 | 235 | 1.611 |
| $C_2H_3-C_6H_5$ | 251↓, 260↑ | 293 | A | 2.367(4) | 1.999(3) | 1.996(3) | 2.521(4) | 4.295 | 279 | 1.453 |
| | | 240 | B | 2.246(4) | 1.980(4) | 2.027(4) | 2.363(5) | 3.357 | 242 | 1.521 |
| | 183↓, 185↑ | 180 | B | 2.263(4) | 1.980(4) | 2.067(4) | 2.398(5) | 3.341 | 238 | 1.516 |
| | | 105 | C | 2.020(6) | 2.245(6) | 2.013(6) | 2.435(7) | 3.360 | 230 | 1.618 |
| 1,3-$(CH_3)_2-C_6H_4$ | 185 | 298 | B | 2.311(3) | 1.961(3) | 1.972(3) | 2.384(4) | 3.475 | 257 | 1.494 |
| | | 240 | B | 2.306(3) | 1.965(2) | 1.981(2) | 2.390(3) | 3.425 | 234 | 1.531 |
| | | 190 | B | 2.284(2) | 1.973(2) | 1.999(2) | 2.415(3) | 3.377 | 229 | 1.551 |
| | | 150 | C | 2.029(2) | 2.203(3) | 2.096(3) | 2.486(1) | 3.358 | 250 | 1.534 |
| | | 120 | C | 1.977(2) | 2.164(3) | 2.057(3) | 2.429(3) | 3.273 | 219 | 1.645 |
| 1-$CH_3$-4-$C_2H_5-C_6H_4$ | 135 | 240 | A | 2.311(3) | 1.980(3) | 1.949(3) | 2.471(3) | 4.204 | 276 | 1.540 |
| | | 150 | A | 2.269(4) | 2.019(4) | 1.958(4) | 2.469(4) | 4.210 | 262 | 1.569 |
| | | 120 | A | 2.219(4) | 2.037(4) | 1.951(4) | 2.442(4) | 4.147 | 244 | 1.613 |
| | | 75 | C | 2.044(6) | 2.268(5) | 1.998(5) | 2.500(6) | 3.549 | 283 | 1.551 |
| 1-$CH_3$-4-$C_2H_3-C_6H_4$ | 125 | 290 | A | 2.338(2) | 1.968(2) | 1.952(2) | 2.537(2) | 4.266 | 282 | 1.513 |
| | | 150 | A | 2.309(2) | 1.994(1) | 1.954(1) | 2.484(2) | 4.190 | 250 | 1.581 |
| | | 100 | C | 2.175(5) | 2.086(5) | 1.969(5) | 2.460(5) | 3.632 | 256 | 1.608 |
| | | 50 | C | 2.017(4) | 2.183(5) | 2.022(5) | 2.464(5) | 3.468 | 251 | 1.624 |
| 1,4-$(CF_3)_2-C_6H_4$ | 117↓, 120↑ | 240 | A | 2.384(2) | 1.963(2) | 1.953(2) | 2.508(2) | 4.254 | 302 | 1.596 |
| | | 120 | A | 2.356(1) | 1.963(1) | 1.955(1) | 2.471(1) | 4.288 | 271 | 1.659 |
| | 50↓, 57↑ | 105 | C | 2.093(2) | 2.112(2) | 2.014(2) | 2.432(2) | 3.718 | 276 | 1.677 |
| | | 65 | C | 2.031(3) | 2.172(3) | 2.015(3) | 2.426(4) | 3.676 | 272 | 1.688 |
| | | 40 | C | 2.063(3) | 2.120(4) | 2.026(4) | 2.415(4) | 3.684 | 267 | 1.694 |
| $C_3H_7-C_6H_5$ | ~105 | 295 | A | 2.343(2) | 1.975(2) | 1.962(2) | 2.510(3) | 4.223 | 296 | 1.507 |
| | | 110 | A | 2.187(3) | 2.112(3) | 1.987(3) | 2.479(3) | 4.127 | 258 | 1.558 |
| | | 100 | A | 2.021(2) | 2.232(2) | 1.950(2) | 2.430(2) | 3.999 | 240 | 1.638 |
| | | 70 | A | 1.978(2) | 2.243(2) | 1.928(2) | 2.397(2) | 3.942 | 223 | 1.692 |
| $C_4H_9-C_6H_5$ | ~120 | 240 | A | 2.325(1) | 1.982(1) | 1.958(1) | 2.510(1) | 4.233 | 287 | 1.533 |
| | | 175 | A | 2.255(2) | 2.031(2) | 1.960(2) | 2.490(2) | 4.187 | 272 | 1.568 |
| | | 125 | A | 2.140(2) | 2.133(2) | 1.962(2) | 2.474(2) | 4.131 | 268 | 1.593 |
| | | 100 | A | 2.032(2) | 2.252(2) | 1.956(2) | 2.462(2) | 4.060 | 268 | 1.610 |
| | | 53 | A | 2.004(1) | 2.284(1) | 1.956(1) | 2.457(2) | 4.025 | 263 | 1.623 |
| 1,4-$(C_2H_5)_2-C_6H_4$ | ~125 | 295 | A | 2.329(2) | 1.967(2) | 1.961(2) | 2.505(2) | 4.278 | 325 | 1.491 |
| | | 240 | A | 2.296(2) | 1.975(2) | 1.969(2) | 2.479(2) | 4.247 | 302 | 1.520 |
| | | 200 | A | 2.268(2) | 1.991(2) | 1.978(2) | 2.478(2) | 4.253 | 286 | 1.536 |
| | | 100 | A | 2.008(2) | 2.062(2) | 2.149(2) | 2.464(2) | 4.247 | 289 | 1.580 |
| | | 50 | A | 1.996(1) | 2.061(2) | 2.162(2) | 2.452(2) | 4.232 | 280 | 1.590 |
| 1,2-$(CH_3)_2-C_6H_4$ | ~150 | 295 | B | 2.285(3) | 1.964(2) | 1.986(2) | 2.397(3) | 3.473 | 244 | 1.516 |
| | | 240 | B | 2.205(3) | 1.975(3) | 2.005(3) | 2.376(4) | 3.351 | 225 | 1.588 |
| | | 180 | B | 2.137(2) | 1.973(2) | 2.110(2) | 2.376(2) | 3.341 | 222 | 1.589 |
| | | 150 | B | 2.064(2) | 1.959(2) | 2.178(2) | 2.373(2) | 3.309 | 210 | 1.631 |
| | | 100 | B | 2.006(2) | 1.951(2) | 2.271(2) | 2.383(2) | 3.281 | 205 | 1.645 |
| | | 60 | B | 2.002(2) | 1.963(2) | 2.301(2) | 2.388(2) | 3.298 | 207 | 1.634 |
| 1,4-$(CH_3)_2-C_6H_4$ | ~200 | 295 | A | 2.329(2) | 1.960(2) | 1.954(2) | 2.480(3) | 4.175 | 264 | 1.529 |
| | | 240 | B | 2.167(3) | 1.981(3) | 2.065(3) | 2.383(3) | 3.339 | 235 | 1.533 |
| | | 200 | B | 2.094(2) | 1.979(2) | 2.152(2) | 2.401(2) | 3.361 | 230 | 1.560 |
| | | 150 | B | 2.004(1) | 1.965(2) | 2.271(2) | 2.406(2) | 3.354 | 220 | 1.594 |
| | | 115 | B | 1.998(2) | 1.964(2) | 2.304(2) | 2.411(2) | 3.358 | 216 | 1.594 |


dx.doi.org/10.1021/ic200444e |*Inorg. Chem.* 2011, 50, 6597–6609

**Table 1. Continued**

| Solv in $Cu(hfac)_2L\cdot 0.5Solv$ | $T_a$ | $T$ | orientation type of solv | $d(Cu-O_{NO})$ | $d(Cu-O_{hfac})$ | $d(Cu-O_{hfac})$ | $d(Cu-N)$ | $d(O_{NO}\cdots O_{NO})$ | $V_{cav}$ | $D_{calcd}$ |
|---|---|---|---|---|---|---|---|---|---|---|
| $1,2,3\text{-}(CH_3)_3-C_6H_3$ | ~150 | 290 | B | 2.269(2) | 1.975(2) | 1.996(2) | 2.420(2) | 3.507 | 264 | 1.501 |
| | | 240 | B | 2.231(2) | 2.000(2) | 2.005(2) | 2.409(2) | 3.473 | 245 | 1.540 |
| | | 142 | B | 2.065(1) | 2.059(2) | 2.093(2) | 2.418(1) | 3.377 | 231 | 1.598 |
| | | 126 | B | 2.035(1) | 2.067(2) | 2.117(2) | 2.419(2) | 3.363 | 230 | 1.606 |
| | | 60 | B | 2.006(2) | 2.060(2) | 2.165(2) | 2.417(2) | 3.320 | 224 | 1.623 |
| $1,2,4\text{-}(CH_3)_3-C_6H_3$ | ~190 | 298 | B | 2.221(2) | 2.013(2) | 1.995(2) | 2.480(2) | 3.531 | 280 | 1.506 |
| | | 240 | B | 2.146(2) | 2.061(2) | 2.017(2) | 2.469(2) | 3.430 | 264 | 1.549 |
| | | 120 | B | 2.014(1) | 2.147(2) | 2.067(2) | 2.450(2) | 3.318 | 236 | 1.609 |
| | | 90 | B | 2.007(1) | 2.154(1) | 2.071(1) | 2.450(2) | 3.309 | 234 | 1.617 |
| $C_6H_6$ | ~45 | 295 | B | 2.332(3) | 1.953(3) | 1.967(3) | 2.393(3) | 3.311 | 198 | 1.526 |
| | | 240 | B | 2.344(3) | 1.932(3) | 1.959(3) | 2.390(3) | 3.302 | 194 | 1.520 |
| | | 150 | B | 2.338(2) | 1.949(2) | 1.976(2) | 2.400(2) | 3.249 | 178 | 1.601 |
| | | 100 | B | 2.334(1) | 1.946(1) | 1.978(1) | 2.402(2) | 3.243 | 173 | 1.624 |
| $CH_3-C_6H_5$ | ~90 | 240 | B | 2.291(2) | 1.944(2) | 1.983(2) | 2.383(3) | 3.328 | 214 | 1.572 |
| | | 120 | B | 2.249(2) | 1.949(2) | 2.048(2) | 2.397(2) | 3.252 | 195 | 1.616 |
| | | 60 | B | 2.101(2) | 1.948(2) | 2.214(2) | 2.406(2) | 3.236 | 195 | 1.626 |
| | | 30 | B | 2.089(2) | 1.946(2) | 2.215(2) | 2.396(2) | 3.204 | 190 | 1.647 |

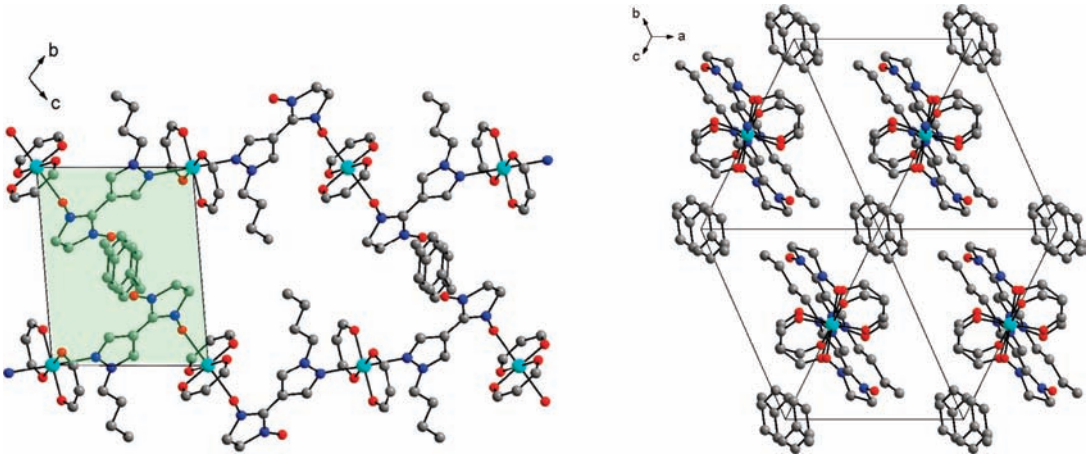


**Figure 1.** Packing of $Cu(hfac)_2L\cdot 0.5CH_3-C_6H_5$ in the high-temperature phase. (Left) View along one of the directions perpendicular to the chains; (right) view along the chains. Here and in all other figures, Cu atoms are shown in cyan, O in red, C in gray, and N in blue. The hydrogen atoms, the geminal methyl groups of L, and the trifluoromethyl groups of the hfac ligands are omitted for clarity.

6.9; F, 28.1. Found: C, 41.9; H, 3.6; N, 6.7; F, 28.0. $Cu(hfac)_2L\cdot 0.5(1,4\text{-}(CH_3)_2-C_6H_4)$: Yield 0.055 g, 70%. Anal. Calcd for $C_{28}H_{30}N_4O_6F_{12}Cu$: C, 41.5; H, 3.7; N, 6.9; F, 28.1. Found: C, 41.6; H, 3.9; N, 6.7; F, 27.9. $Cu(hfac)_2L\cdot 0.5(1,4\text{-}(CF_3)_2-C_6H_4)$: Yield 0.065 g, 80%. Anal. Calcd for $C_{28}H_{27}N_4O_6F_{15}Cu$: C, 38.9; H, 3.2; N, 6.5; F, 33.0. Found: C, 38.4; H, 3.5; N, 6.5; F, 32.8. $Cu(hfac)_2L\cdot 0.5(1\text{-}CH_3\text{-}4\text{-}C_2H_5-C_6H_4)$: Yield 0.055 g, 75%. Anal. Calcd for $C_{28.5}H_{31}N_4O_6F_{12}Cu$: C, 41.9; H, 3.8; N, 6.9; F, 27.9. Found: C, 41.7; H, 4.2; N, 6.5; F, 27.9. $Cu(hfac)_2L\cdot 0.5(1\text{-}CH_3\text{-}4\text{-}C_2H_3-C_6H_4)$: Yield 0.030 g, 39%. Anal. Calcd for $C_{28.5}H_{30}N_4O_6F_{12}Cu$: C, 41.9; H, 3.7; N, 6.9; F, 27.9. Found: C, 42.1; H, 3.7; N, 6.5; F, 27.7. $Cu(hfac)_2L\cdot 0.5(1,4\text{-}(C_2H_5)_2-C_6H_4)$: Yield 0.055 g, 71%. Anal. Calcd for $C_{29}H_{32}N_4O_6F_{12}Cu$: C, 42.3; H, 3.9; N, 6.8; F, 27.7. Found: C, 42.6; H, 4.2; N, 6.9; F, 28.0. $Cu(hfac)_2L\cdot 0.5(1,2,3\text{-}(CH_3)_3-C_6H_3)$: Yield 0.050 g, 66%. Anal. Calcd for $C_{28.5}H_{31}N_4O_6F_{12}Cu$: C, 41.9; H, 3.8; N, 6.9; F, 27.9. Found: C, 41.6; H, 3.9; N, 6.7; F, 27.6. $Cu(hfac)_2L\cdot 0.5(1,2,4\text{-}(CH_3)_3-C_6H_3)$: Yield 0.065 g, 85%. Anal. Calcd for $C_{28.5}H_{31}N_4O_6F_{12}Cu$: C, 41.9; H, 3.8; N, 6.9; F, 27.9. Found: C, 41.5; H, 3.8; N, 6.6; F, 27.7.

**X-ray Crystallography.** The intensity data for the single crystals of the compounds were collected on a SMART APEX CCD (Bruker AXS) automated diffractometer with a Helix (Oxford Cryosystems) open-flow helium cooler using the standard procedure (Mo Kα radiation). The structures were solved by direct methods and refined by the full-matrix least-squares procedure anisotropically for non-hydrogen atoms. The H atoms were partially located in difference electron density syntheses, and the others were calculated geometrically and included in the refinement as riding groups. All calculations were fulfilled with the SHELXTL 6.14 program package. The temperature dynamics of the selected structural parameters for $Cu(hfac)_2L\cdot 0.5Solv$ is presented in Table 1.

## RESULTS AND DISCUSSION

Previous studies of a number of isostructural solvates with acyclic solvents (pentane, hexane, heptane, and octane) showed that the natural homologous unit of one methylene group was too large to change the magnetic effect in breathing crystals.[13] A superposition of the experimental dependences $\mu_{eff}(T)$ for solvates with these solvent molecules clearly showed that the magnetic anomalies differed in the temperature, range, and abruptness between solvates.[13,29] This is completely confirmed by the data of this study for aromatic solvates. Moreover, the data


dx.doi.org/10.1021/ic200444e |*Inorg. Chem.* 2011, 50, 6597–6609

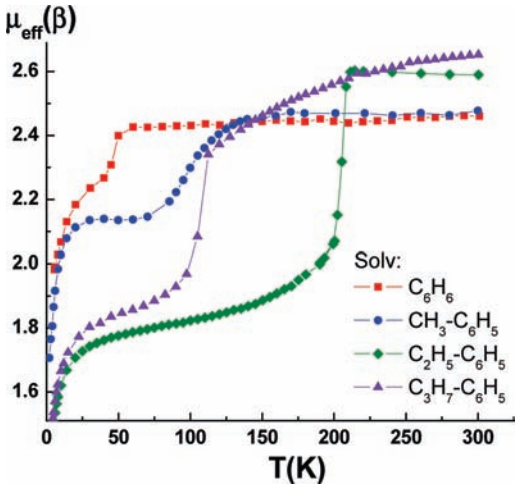


**Figure 2.** Temperature dependences of the effective magnetic moment of $Cu(hfac)_2L\cdot 0.5C_6H_6$ (red), $Cu(hfac)_2L\cdot 0.5CH_3-C_6H_5$ (blue), $Cu(hfac)_2L\cdot 0.5C_2H_5-C_6H_5$ (green), and $Cu(hfac)_2L\cdot 0.5C_3H_7-C_6H_5$ (violet).

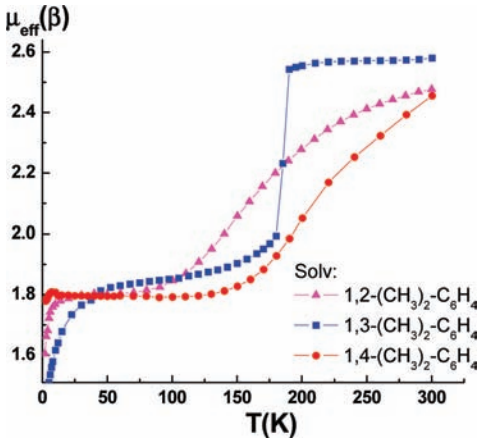


**Figure 3.** Temperature dependences of the effective magnetic moment of $Cu(hfac)_2L\cdot 0.5(1,2\text{-}(CH_3)_2-C_6H_4)$ (magenta), $Cu(hfac)_2L\cdot 0.5(1,3\text{-}(CH_3)_2-C_6H_4)$ (blue), and $Cu(hfac)_2L\cdot 0.5(1,4\text{-}(CH_3)_2-C_6H_4)$ (red).

given below actually show that the magnetic characteristics of breathing crystals are sensitive not only to the slightest changes in the structure and composition of solvent guest molecules but also to variation of their orientation relative to the paramagnetic fragments. Initially, we could hardly admit that the temperature and character of the magnetic anomaly on the $\mu_{eff}(T)$ curve could react so strongly to rotations of solvate molecules in the intracrystalline space of $Cu(hfac)_2L\cdot 0.5Solv$ because there were no interactions between the $\{Cu(hfac)_2L\}_\infty$ heterospin polymer chains and the Solv guest molecules except van der Waals interactions. Therefore, only a detailed analysis of the thermally induced reorientations of aromatic solvate molecules in $Cu(hfac)_2L\cdot 0.5Solv$ crystals allowed a systematization of experimental data from a single viewpoint, although the data initially seemed rather disembodied.

Let us consider the data for $Cu(hfac)_2L\cdot 0.5Solv$, where Solv is benzene, toluene, ethylbenzene, or propylbenzene. For these and all other solvates, the crystal structures are isotypical, that is, the

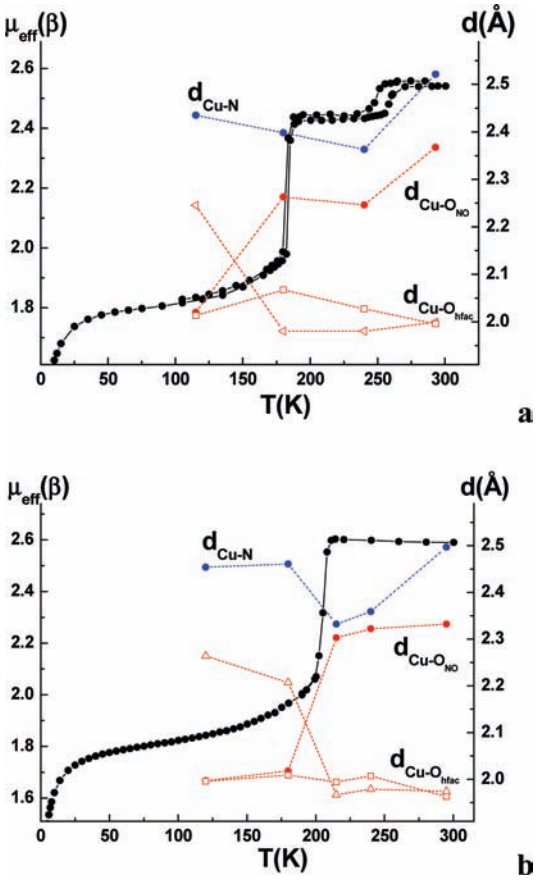


**Figure 4.** Temperature dependences of the effective magnetic moment and Cu−N and $Cu-O_{NO}$ bond lengths at different temperatures for $Cu(hfac)_2L\cdot 0.5C_2H_5-C_6H_5$ (a) and $Cu(hfac)_2L\cdot 0.5C_2H_5-C_6H_5$ (b); for explanations, see the text.

chain packing and solvent localization are similar. Figure 1 shows the packing of $Cu(hfac)_2L\cdot 0.5CH_3-C_6H_5$ as an example. It can be seen that the $CuO_4$ square environment in the coordination matrices of $Cu(hfac)_2$ is completed to a distorted octahedron either by two N atoms of the pyrazole rings of two bridging bidentate ligands L or by two $O_{NO}$ atoms of the nitronyl nitroxyl fragments. The second O atom of the nitronyl nitroxyl fragment is not involved in the coordination. As a result, the Cu(II) ions lying in the $CuN_2O_4$ coordination units alternate with the $>N-^{\bullet}O-Cu^{II}-O^{\bullet}-N<$ heterospin clusters of the $CuO_6$ units in the "head-to-head" chains. Figure 2 shows that for solvates with benzene, toluene, ethylbenzene, and propylbenzene whose molecules formally differ by only one methylene unit both the range and the temperature of the magnetic anomaly differ widely. For solvates with benzene and toluene, the abrupt decrease in $\mu_{eff}$ corresponds to a decrease from 3/2 to 1/2 in the total number of spins in approximately one-half of all $>N-^{\bullet}O-Cu^{II}-O^{\bullet}-N<$ exchange clusters. For solvates with ethylbenzene and propylbenzene, however, a decrease by a factor of $\sqrt{2}$ in $\mu_{eff}$ from high- to low-temperature phase corresponds to a decrease to 1/2 in the total number of spins in all $>N-^{\bullet}O-Cu^{II}-O^{\bullet}-N<$ exchange clusters. The magnetic anomaly temperatures ($T_a$) also differ significantly: 45 ± 3, 90 ± 3, 103 ± 3, and 205 ± 3 K for $Cu(hfac)_2L\cdot 0.5C_6H_6$, $Cu(hfac)_2L\cdot 0.5CH_3-C_6H_5$, $Cu(hfac)_2L\cdot 0.5C_3H_7-C_6H_5$, and $Cu(hfac)_2L\cdot 0.5C_2H_5-C_6H_5$, respectively. These series of $T_a$ cannot be reasonably correlated


dx.doi.org/10.1021/ic200444e |Inorg. Chem. 2011, 50, 6597–6609

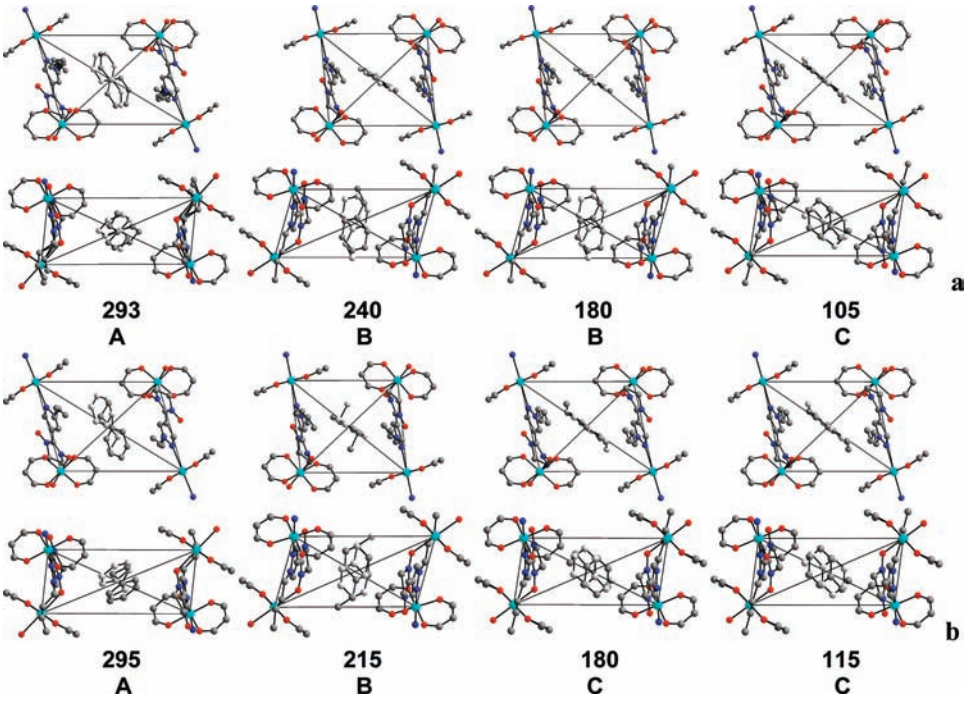


**Figure 5.** Variation of the orientation of the styrene solvate molecule (a) and ethylbenzene (b) at different temperatures (for description, see the text).

with the change in the composition of the solvate molecule. The reasons for the differences in the high-temperature asymptotics of $\mu_{eff}$ are also not clear (Figure 2).

If we compare the dependences $\mu_{eff}(T)$ for solvates with *o*-xylene, *p*-xylene, and *m*-xylene (Figure 3), the temperatures and forms of the effect are different again, although its range is the same ($\mu_{eff}$ decreases by a factor of $\sqrt{2}$). In other words, the structural rearrangement of the breathing crystal in general and hence the form of the magnetic anomaly are sensitive to the spatial arrangement of the methyl substituents in xylene molecules, which is almost the same if they are rotated around the axis through the center of the benzene ring. A more detailed study of the magnetic structural anomalies of $Cu(hfac)_2L\cdot 0.5Solv$ showed that the thermally induced intracrystalline rearrangements allow only definite orientations of the aromatic rings and substituents in them relative to the heterospin chains. Each of these orientations, in turn, determines the character of exchange interactions in $>N-^{\bullet}O-Cu^{II}-O^{\bullet}-N<$ exchange clusters.

Let us consider the thermally induced dynamics of exchange clusters and the coupled magnetic effects for the $Cu(hfac)_2L\cdot 0.5C_2H_3-C_6H_5$ solvate with styrene. The $\mu_{eff}(T)$ curve in Figure 4a shows two abrupt changes corresponding to a very narrow hysteresis loop at a low temperature ($T^1_a\uparrow = 185$ K, $T^1_a\downarrow = 183$ K) and a wider one at high temperature ($T^2_a\uparrow = 260$ K, $T^2_a\downarrow = 251$ K). The same figure gives the Cu−N and Cu−O bond lengths for $Cu(hfac)_2L\cdot 0.5C_2H_3-C_6H_5$ at 105, 180, 240, and 293 K; these values along with other selected structural parameters for $Cu(hfac)_2L\cdot 0.5C_2H_3-C_6H_5$ and other $Cu(hfac)_2L\cdot 0.5Solv$ are also given in Table 1. The temperatures 105, 180, 240, and 293 K correspond to the $\mu_{eff}$ values above and below the region of anomalies. The blue dashed lines connect the values of bond lengths between the Cu atoms and the coordinated imine N atoms of the pyrazole rings ($d$(Cu−N), blue full circles in Figure 4a), demonstrating the dynamics of changes in the interatomic distances at different temperatures. The red dashed lines connect the dots corresponding to the bond lengths between the Cu atoms and the coordinated O atoms of the nitroxyl groups ($d(Cu-O_{NO})$, red full circles) and hexafluoroacetylacetonate anions ($d(Cu-O_{hfac})$, red open squares and triangles) at the same temperatures. According to the plots, the magnetic anomaly is accompanied by significant changes in the $CuO_6$ coordination units at each stage. When the temperature was lowered from 293 to 240 K, the distances $d(Cu-O_{NO})$ decreased from 2.367(4) to 2.246(4) Å. The stage corresponding to the decrease in temperature from 180 to 105 K was accompanied by a further decrease in $d(Cu-O_{NO})$ from 2.263(4) to 2.020(6) Å. The $d(Cu-O_{hfac})$ distances increased significantly from 1.999(3) to 2.245(6) Å along one of the axes in the $CuO_6$ units. $Cu(hfac)_2L\cdot 0.5C_2H_3-C_6H_5$ thus undergoes two phase transitions at lowered temperatures, leading to a change in the Jahn−Teller axis in all $CuO_6$ coordination units of the low-temperature phase of $Cu(hfac)_2L\cdot 0.5C_2H_3-C_6H_5$. All nitroxyl O atoms pass from axial to equatorial positions. This is favorable for the formation of a low-spin state in the $>N-^{\bullet}O-Cu^{II}-O^{\bullet}-N<$ spin triads, which, in turn, leads to a complete coupling of one-half of all spins and decreases $\mu_{eff}$ by a factor of $\sqrt{2}$.[1,7−11,13,29] A small change in $\mu_{eff}$ at 240−260 K corresponding to the 9 K wide hysteresis loop (recorded during repeated cooling−heating cycles) is due to the structural rearrangement in the exchange triads. According to quantum-chemical data,[2,13,17,23−25,48] the shortening of the distances between the paramagnetic centers $d(Cu-O_{NO})$ decreases the ferromagnetic contribution to the exchange interaction but increases the antiferromagnetic contribution. As a result, the effective magnetic moment decreases. Curiously, the distances $d$(Cu−N) in the $CuN_2O_4$ units are shortened significantly (from 2.521(4) to 2.363(5) Å) when the temperature is lowered from 293 to 240 K but lengthened again (to 2.435(7) Å) after cooling to 105 K.

Temperature variation leads not only to changes in the Cu−N and Cu−O distances in the coordination units of solid


dx.doi.org/10.1021/ic200444e |*Inorg. Chem.* 2011, 50, 6597–6609

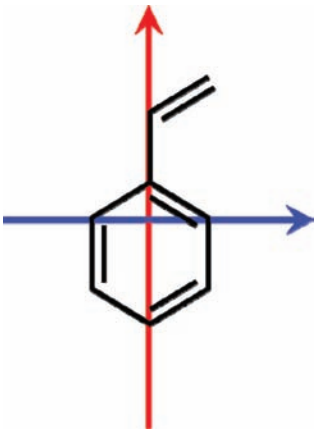

**Figure 6.** Plane of the aromatic ring of the styrene molecule and position of the vinyl group (orthogonal arrows).

$Cu(hfac)_2L\cdot 0.5C_2H_3-C_6H_5$ but also to numerous concerted motions of atoms in polymer chains and to mutual displacements of the chains and the interchain styrene molecules in the breathing crystal. An analysis of a large data set showed that each plateau on the $\mu_{eff}(T)$ curve for $Cu(hfac)_2L\cdot 0.5C_2H_3-C_6H_5$ corresponded to a definite orientation of styrene molecules in crystal denoted as A, B, or C in Figure 5a. This is vividly demonstrated by two projections of the structure of $Cu(hfac)_2L\cdot 0.5C_2H_3-C_6H_5$ at 105, 180, 240, and 293 K corresponding to $\mu_{eff}$ above and below the anomaly regions. In Figure 5a the first line presents projections along the planes of the $CuO_4$ chelate units of the $Cu(hfac)_2$ coordination matrices lying in the top left and bottom right corners of the parallelogram; the second line shows projections viewed along the planes of the $CuO_4$ chelate units of the $Cu(hfac)_2$ coordination matrices lying in the top right and bottom left corners of the parallelogram. The diagonals of the parallelograms show the orientations of solvent molecules relative to them and to the center of the parallelogram.

To represent the dynamics of the solvent molecule relative to the polymer chains at different temperatures more clearly and correlate this dynamics with changes in the magnetic properties of the compounds, in Figure 6 we drew two (red and blue) mutually orthogonal arrows related to the aromatic ring of the styrene molecule chosen as an example. The red arrow passes through the C atom of the *para*-position and the C atom to which the vinyl group is bonded. The blue arrow passes through both C atoms in the *ortho*-position relative to the C atom to which the vinyl group is bonded. A change in the direction of these arrows in Figure 7 allows us to represent the reorientation of the styrene molecule in the interchain space at different temperatures. The black line that connects the copper atoms (Figure 7) corresponds to the overlapping sides of the parallelogram shown in Figure 1 (left) if viewed from the left. At $T > 260$ K (Figure 7, orientation A), the styrene molecule lies almost in the plane of the polymer chains. The plane of the aromatic ring of the styrene molecule lies at an angle of ~16° relative to the plane of the parallelogram isolated in Figure 1. A phase transition accompanied by a reorientation of the styrene molecule occurs at lower temperatures at the intersection with the region 260−251 K. It deviates from the chosen plane of chains. The aromatic ring then lies at an angle of ~65° relative to the plane of the parallelogram (orientation B), i.e., to the chosen plane of polymer chains.

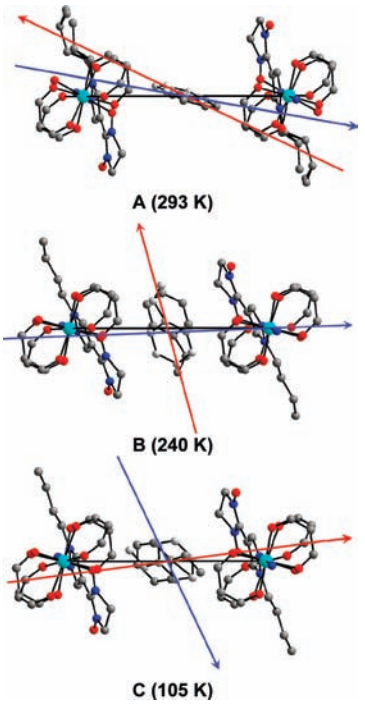


**Figure 7.** Reorientations of the styrene molecule in the interchain space at different temperatures. See text for details.

The direction of the red arrow corresponds to the direction of the vinyl substituents in the intracrystalline space. Another structural rearrangement occurs below 180 K and is accompanied by another reorientation of the styrene molecule relative to the polymer chains (Figure 7, orientation C). The styrene molecule then rotates clockwise, which is clearly seen from a comparison of the directions of the red and blue arrows for orientations B and C in Figure 7. The angle between the plane of the aromatic ring of the styrene molecule and the plane of the chains is almost constant (~61°). These orientations of solvent molecules are discussed below and summarized in Table 2.

It appeared that using the A, B, and C generalized orientations of Solv molecules in solid $Cu(hfac)_2L\cdot 0.5$Solv provided a clue to the magnetochemical behavior of solvates with different solvent molecules. This is confirmed by Figure 8, which shows the $\mu_{eff}(T)$ dependence for $Cu(hfac)_2L\cdot 0.5C_2H_3-C_6H_5$ as a reference for comparing it with $\mu_{eff}(T)$ for $Cu(hfac)_2L\cdot 0.5C_2H_5-C_6H_5$ and $Cu(hfac)_2L\cdot 0.5(1,3\text{-}(CH_3)_2-C_6H_4)$.

A comparison of the $\mu_{eff}(T)$ dependences for $Cu(hfac)_2L\cdot 0.5C_2H_3-C_6H_5$ and $Cu(hfac)_2L\cdot 0.5C_2H_5-C_6H_5$ shows that the high- (>260 K) and low-temperature (<170 K) asymptotics of $\mu_{eff}(T)$ coincide very closely for these solvates. This means that the solvent molecules in these solvates are orientated according to type A at room temperature and type C at low temperatures. The same conclusion is drawn if we compare the structural solutions at different temperatures shown in Figure 5a and 5b for $Cu(hfac)_2L\cdot 0.5C_2H_3-C_6H_5$ and $Cu(hfac)_2L\cdot 0.5C_2H_5-C_6H_5$. The types of orientation of the aromatic solvent in solid $Cu(hfac)_2L\cdot 0.5C_2H_3-C_6H_5$ and $Cu(hfac)_2L\cdot 0.5C_2H_5-C_6H_5$ proved the same. It is therefore quite logical that the high- (>260 K) and low-temperature (<170 K) asymptotics of $\mu_{eff}(T)$ should be similar for these solvates. The only question is why is the A ⇆ B phase transition not visible on the $\mu_{eff}(T)$ curve for $Cu(hfac)_2L\cdot 0.5C_2H_5-C_6H_5$? The answer


dx.doi.org/10.1021/ic200444e |*Inorg. Chem.* 2011, 50, 6597–6609

**Table 2. Types of Transitions**

| | |
|---|---|
| 1) $A_{LS} \leftrightarrows A_{HS}$ (magenta-colored in Figure 13) | A |
| 2) $C_{LS} \leftrightarrows A_{HS}$ (blue-colored in Figure 13) | |
| 3) $B_{LS} \leftrightarrows B_{HS}$ (orange-colored in Figure 13) | B |
| 4) $C_{LS} \leftrightarrows B_{HS}$ and/or $C_{LS} \leftrightarrows B_{HS} \leftrightarrows A_{HS}$ (green-colored in Figure 13) | |

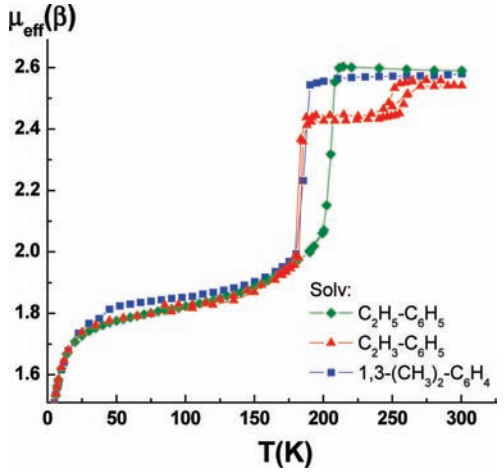


**Figure 8.** Temperature dependences of the effective magnetic moment of $Cu(hfac)_2L\cdot 0.5C_2H_3-C_6H_5$ (red), $Cu(hfac)_2L\cdot 0.5C_2H_5-C_6H_5$ (green), and $Cu(hfac)_2L\cdot 0.5(1,3\text{-}(CH_3)_2-C_6H_4)$ (blue).

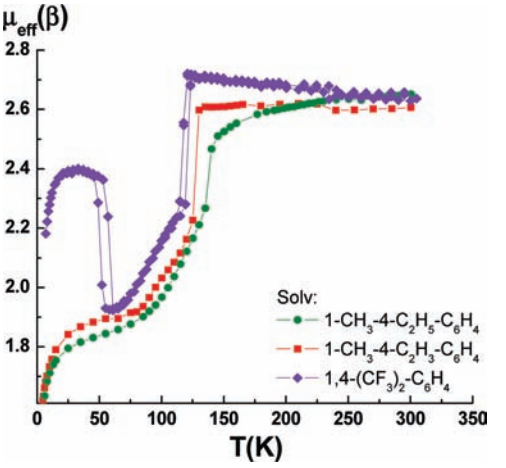


**Figure 9.** Temperature dependences of the effective magnetic moment of $Cu(hfac)_2L\cdot 0.5(1,4\text{-}(CF_3)_2-C_6H_4)$ (violet), $Cu(hfac)_2L\cdot 0.5(1\text{-}CH_3\text{-}4\text{-}C_2H_3-C_6H_4)$ (red), and $Cu(hfac)_2L\cdot 0.5(1\text{-}CH_3\text{-}4\text{-}C_2H_5-C_6H_4)$ (green).

can readily be found if we compare the dynamics of changes in the Cu−N and Cu−O interatomic distances in $Cu(hfac)_2L\cdot 0.5C_2H_3-C_6H_5$ and $Cu(hfac)_2L\cdot 0.5C_2H_5-C_6H_5$ at different temperatures (Figure 4a and 4b). When the temperature lowered from room temperature to ~205 K (Table 1) in solid $Cu(hfac)_2L\cdot 0.5C_2H_5-C_6H_5$, the Cu−N distances shortened considerably, while the $Cu-O_{NO}$ distances changed very insignificantly in the course of the structural transformation accompanied by an A→B-type reorientation of the solvent. For $Cu(hfac)_2L\cdot 0.5C_2H_3-C_6H_5$, however, the case was different. As mentioned above, the changes in the $Cu-O_{NO}$ distances in the $>N-^{\bullet}O-Cu^{II}-O^{\bullet}-N<$ exchange clusters of $Cu(hfac)_2L\cdot 0.5C_2H_3-C_6H_5$ are responsible for the effect recorded at 250−260 K for this compound. Since the A→B reorientation in solid $Cu(hfac)_2L\cdot 0.5C_2H_5-C_6H_5$ does not affect the $CuO_6$ units, there should be no anomalies on the $\mu_{eff}(T)$ curve on cooling the compound to ~205 K. Further cooling of $Cu(hfac)_2L\cdot 0.5C_2H_5-C_6H_5$ crystals caused a drastic shortening of $Cu-O_{NO}$ distances, giving rise to an anomaly on the $\mu_{eff}(T)$ curve, namely, a decrease in the effective magnetic moment. This anomaly structurally corresponds to the B→C transformation.

As shown by our X-ray diffraction study of the solvate with *m*-xylene, the structural dynamics in $Cu(hfac)_2L\cdot 0.5(1,3\text{-}(CH_3)_2-C_6H_4)$ crystals on cooling corresponds to type B(298, 240, 190 K) → C(150, 120 K). The figures after the B and C symbols of orientations in parentheses are the temperatures at which the crystal structure was solved. The temperatures of the X-ray diffraction experiment are also listed in the third column of Table 1. The second and fourth columns give the values of $T_a$ and the types of the orientation of solvent molecules for all $Cu(hfac)_2L\cdot 0.5$Solv compounds.

The form of the magnetic effect and the temperature asymptotics for $Cu(hfac)_2L\cdot 0.5(1,3\text{-}(CH_3)_2-C_6H_4)$ on the $\mu_{eff}(T)$ curve are close to those for the solvate with ethylbenzene (Figure 8). The similarity between the $\mu_{eff}(T)$ curves for solvates with *m*-xylene and ethylbenzene is not surprising (Figure 8). The $Cu-O_{NO}$ distances change very insignificantly up to the transition temperatures, and the $d(Cu-O_{NO})$ values are close for the solvates (Table 1).

The spatial analysis data for $Cu(hfac)_2L\cdot 0.5(1,3\text{-}(CH_3)_2-C_6H_4)$ similar to the data for $Cu(hfac)_2L\cdot 0.5C_2H_3-C_6H_5$ and $Cu(hfac)_2L\cdot 0.5C_2H_5-C_6H_5$ are given in Figures S1 and S2 in the Supporting Information. Note that for $Cu(hfac)_2L\cdot 0.5(1,3\text{-}(CH_3)_2-C_6H_4)$, the A structural type of the solvate was not recorded at all; the results of high-temperature studies at 298, 240, and 190 K corresponded to the B structural type (Table 1). Indeed, the high-temperature values of $d(Cu-N)$ given in Table 1 are close to those for $Cu(hfac)_2L\cdot 0.5C_2H_3-C_6H_5$ and $Cu(hfac)_2L\cdot 0.5C_2H_5-C_6H_5$ after the A→B transition. For the B→A transition, however, the $Cu(hfac)_2L\cdot 0.5(1,3\text{-}(CH_3)_2-C_6H_4)$ sample could not be heated above 325 K because it started to decompose.

The above discussion concerned the solvates for which the transitions between the spin states abruptly occurred at ~180−200 K. Among the compounds under study was another group of aromatic solvates, for which the transitions between the spin states were also clear cut but observed in a different range


dx.doi.org/10.1021/ic200444e |*Inorg. Chem.* 2011, 50, 6597–6609

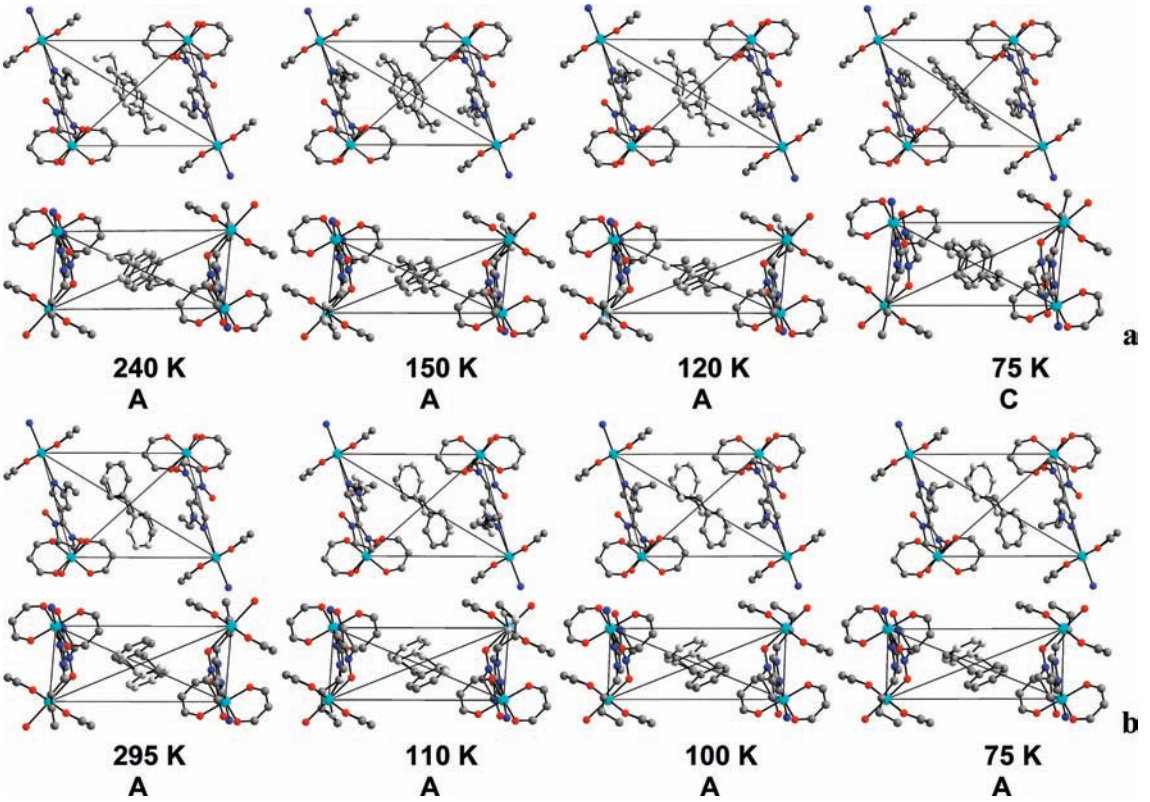


**Figure 10.** A→C reorientation of the solvate molecule in solid $Cu(hfac)_2L\cdot 0.5(1\text{-}CH_3\text{-}4\text{-}C_2H_5{-}C_6H_4)$ on cooling (a), and absence of solvent reorientation in $Cu(hfac)_2L\cdot 0.5C_3H_7{-}C_6H_5$ (b).

at ~115−135 K (Figure 9). These are solvates with 1,4-bis-(trifluoromethyl)benzene, 1-methyl-4-vinylbenzene, and 1-methyl-4-ethylbenzene. The dependences $\mu_{eff}(T)$ for them are very much alike except the low-temperature range (<60 K) for the complex with 1,4-bis(trifluoromethyl)benzene (Figure 9). Indeed, they should be attributed to the same type if we consider the orientation of the aromatic solvent in solids. As the transition temperature decreases while $\mu_{eff}$ changes abruptly, the solvent molecules undergo the A→C reorientation. This is supported by an example in Figure 10a, which shows the fragments of the structure of $Cu(hfac)_2L\cdot 0.5(1\text{-}CH_3\text{-}4\text{-}C_2H_5{-}C_6H_4)$ at different temperatures. A comparison of the reorientation types of the solvent molecule in the solid solvate with similar data for $Cu(hfac)_2L\cdot 0.5C_2H_3{-}C_6H_5$ and $Cu(hfac)_2L\cdot 0.5C_2H_5{-}C_6H_5$ (Figure 5) shows that the 1-methyl-4-ethylbenzene molecules undergo the A to C reorientation avoiding the B orientation. Similar illustrations, demonstrating the reorientation of the 1,4-bis(trifluoromethyl)benzene solvate molecule in $Cu(hfac)_2L\cdot 0.5(1,4\text{-}(CF_3)_2{-}C_6H_4)$ or 1-methyl-4-vinylbenzene in $Cu(hfac)_2L\cdot 0.5(1\text{-}CH_3\text{-}4\text{-}C_2H_3{-}C_6H_4)$ at different temperatures, are given in the Supporting Information (Figure S3).

The increase in the $\mu_{eff}$ of $Cu(hfac)_2L\cdot 0.5(1,4\text{-}(CF_3)_2{-}C_6H_4)$ below 50 K requires a separate comment (Figure 9). Figure 11a shows the $\mu_{eff}(T)$ dependence for $Cu(hfac)_2L\cdot 0.5(1,4\text{-}(CF_3)_2{-}C_6H_4)$ in comparison with the temperature dependences of the Cu−N and $Cu{-}O_{NO}$ bond lengths. As in Figure 4, the blue dashed lines connect the values of the Cu−N bond lengths between the Cu atoms and the coordinated imine N atoms of the pyrazole rings; the red dashed lines link the points corresponding to the $Cu{-}O_{NO}$ bond lengths between the Cu atoms and the coordinated O atoms of the nitroxyl groups ($d(Cu{-}O_{NO})$, full red circles) and $Cu{-}O_{hfac}$ bond lengths of the hexafluoroacetylacetonate anions ($d(Cu{-}O_{hfac})$, open squares and red triangles). Figure 11a demonstrates two important circumstances. First, after a drastic decrease in $\mu_{eff}$ at 117 K, further cooling of the solvate to 60 K causes a smoother decrease in the effective magnetic moment. According to the structural data for $Cu(hfac)_2L\cdot 0.5(1,4\text{-}(CF_3)_2{-}C_6H_4)$ at 105 and 65 K, after the A→C structural transition, the low-temperature phase is simply compressed and the Cu−N and $Cu{-}O_{NO}$ bonds are shortened further (Table 1). Similar tendencies for these bonds were also recorded for $Cu(hfac)_2L\cdot 0.5(1\text{-}CH_3\text{-}4\text{-}C_2H_3{-}C_6H_4)$ and $Cu(hfac)_2L\cdot 0.5(1\text{-}CH_3\text{-}4\text{-}C_2H_5{-}C_6H_4)$ (Figure S4, Supporting Information). For solid $Cu(hfac)_2L\cdot 0.5(1,4\text{-}(CF_3)_2{-}C_6H_4)$, however, the $Cu{-}O_{hfac}$ bond lengths ceased to increase but started to decrease in the range 105−65 K. At 40 K the X-ray diffraction study revealed a still more pronounced decrease in the $Cu{-}O_{hfac}$ bond lengths and a shift toward an increase in the $Cu{-}O_{NO}$ bond lengths.

The latter tendency toward increasing $Cu{-}O_{NO}$ bond lengths at very low temperatures is very important because the increase in $\mu_{eff}$ at $T$ < 60 K can only be explained by the appearance of $>N{-}^{\bullet}O{-}Cu^{II}{-}O^{\bullet}{-}N<$ exchange clusters with reasonably long $Cu{-}O_{NO}$ distances favorable for the ferromagnetic exchange.[2,13,17,23−25,48] Note also that hysteresis loops were found at low ($T^1_a\uparrow$ = 57 K, $T^1_a\downarrow$ = 50 K) and higher ($T^2_a\uparrow$ = 120 K, $T^2_a\downarrow$ = 117 K) temperatures in the transition region on the $\mu_{eff}(T)$ curve when the cooling−heating cycles were repeated (Figure 11a). The abrupt increase in $\mu_{eff}(T)$ at lower temperatures is a very rare anomaly observed in studies of spin transitions.[4,10,13,49]


dx.doi.org/10.1021/ic200444e |*Inorg. Chem.* 2011, 50, 6597–6609

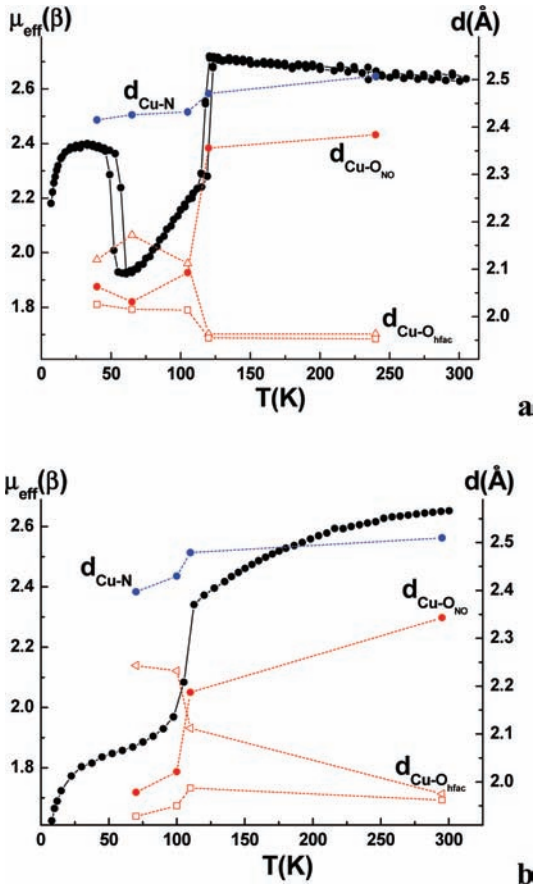


**Figure 11.** Temperature dependences of the effective magnetic moment and the Cu−N and Cu−$O_{NO}$ bond lengths at different temperatures for Cu(hfac)$_2$L·0.5(1,4-(CF$_3$)$_2$−C$_6$H$_4$) (a) and Cu(hfac)$_2$L·0.5C$_3$H$_7$−C$_6$H$_5$ (b); see text for explanations.

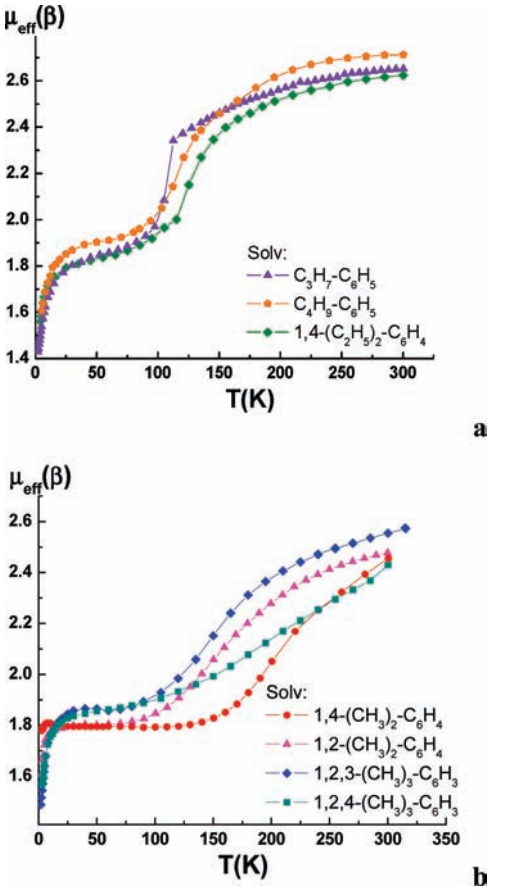


**Figure 12.** Temperature dependences of the effective magnetic moment of Cu(hfac)$_2$L·0.5Solv, where Solv = C$_3$H$_7$−C$_6$H$_5$ (violet triangles), C$_4$H$_9$−C$_6$H$_5$ (orange pentagons), and 1,4-(C$_2$H$_5$)$_2$−C$_6$H$_4$ (green diamonds) (a) and of Cu(hfac)$_2$L·0.5Solv, where Solv = 1,2-(CH$_3$)$_2$−C$_6$H$_4$ (magenta triangles), 1,4-(CH$_3$)$_2$−C$_6$H$_4$ (red circles), 1,2,3-(CH$_3$)$_3$−C$_6$H$_3$ (blue diamonds), and 1,2,4-(CH$_3$)$_3$−C$_6$H$_3$ (cyan squares) (b).

Studies of magnetostructural correlations inherent in Cu(hfac)$_2$L·0.5Solv revealed another two groups of compounds similar in the temperature range of the magnetic anomaly and in the type of structural organization of the solid phase. One of the groups includes Cu(hfac)$_2$L·0.5C$_3$H$_7$−C$_6$H$_5$, Cu(hfac)$_2$L·0.5C$_4$H$_9$−C$_6$H$_5$, and Cu(hfac)$_2$L·0.5(1,4-(C$_2$H$_5$)$_2$−C$_6$H$_4$), having longer alkyl substituents in the benzene ring of solvate molecules than the above-discussed compounds. Their smooth transition from the high- to the low-spin state occurs in the range ∼100−140 K (Figure 12a). The smoothness of the transition fully agrees with the structural data. An XRD study of solvates with propylbenzene, butylbenzene, and 1,4-diethylbenzene showed that their structural organization remained constant in the chosen representation. It corresponded to type A over the whole temperature range, i.e., in the temperature range of the magnetic anomaly as well as above and below it (Table 1; Figure 10b; Figure S5, Supporting Information). The structural parameters of heterospin chains that bypass the solvent guest molecules (Table 1) changed, but the orientation of the solvent molecules did not. Figure 11b shows that $\mu_{eff}$ changed symbatically with the structural parameters of Cu(hfac)$_2$L·0.5C$_3$H$_7$−C$_6$H$_5$. The structural parameters of Cu(hfac)$_2$L·0.5C$_4$H$_9$−C$_6$H$_5$ and Cu(hfac)$_2$L·0.5(1,4-(C$_2$H$_5$)$_2$−C$_6$H$_4$) changed similarly to those of Cu(hfac)$_2$L·0.5C$_3$H$_7$−C$_6$H$_5$ at different temperatures (Figures S5 and S6, Supporting Information). The rearrangement of the solvates at lowered temperatures in general can be represented in the following way. The orientation of the solvent guest molecules remains constant, while the bypassing heterospin chains are shortened. The fraction of the low-temperature phase increases, and the antiferromagnetic exchange dominates in the phase due to the shortening of the Cu−$O_{NO}$ bond lengths in >N−$^{\bullet}$O−Cu$^{II}$−O$^{\bullet}$−N< exchange clusters.[13,23] In contrast, when Cu(hfac)$_2$L·0.5C$_3$H$_7$−C$_6$H$_5$, Cu(hfac)$_2$L·0.5C$_4$H$_9$−C$_6$H$_5$, and Cu(hfac)$_2$L·0.5(1,4-(C$_2$H$_5$)$_2$−C$_6$H$_4$) are heated, the Cu−$O_{NO}$ bond lengths increase; as a consequence, the fraction of >N−$^{\bullet}$O−Cu$^{II}$−O$^{\bullet}$−N< high-spin clusters in the solid solvate also increases.[23]

Similar magnetostructural correlations were recorded for another group of solvates with *o*-xylene, *p*-xylene, 1,2,3-trimethylbenzene, and 1,2,4-trimethylbenzene, namely, Cu(hfac)$_2$L·0.5(1,2-(CH$_3$)$_2$−C$_6$H$_4$), Cu(hfac)$_2$L·0.5(1,4-(CH$_3$)$_2$−C$_6$H$_4$), Cu(hfac)$_2$L·0.5(1,2,3-(CH$_3$)$_3$−C$_6$H$_3$), and Cu(hfac)$_2$L·0.5(1,2,4-(CH$_3$)$_3$−C$_6$H$_3$). The only difference between these and the above-described solvates lies in the fact that the transition from low to high $\mu_{eff}$ values occurs in another temperature range, ∼150−300 K (Figure 12b), because the constant structural organization of these solvates corresponds to type B over the whole temperature range. The experimental evidence for this is presented in the Supporting Information (Figures S7−S10). These results are logically similar to


dx.doi.org/10.1021/ic200444e |*Inorg. Chem.* 2011, 50, 6597–6609

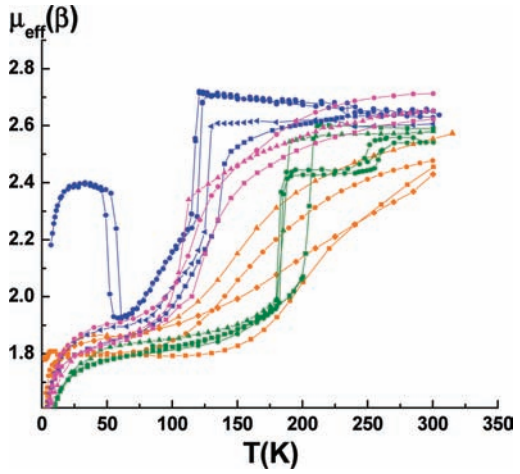


**Figure 13.** Superposition of the "abrupt" anomalies $C_{LS} \leftrightarrows A_{HS}$ (blue dots connected by blue lines) on the smooth anomalies $A_{LS} \leftrightarrows A_{HS}$ (sets of experimental points and connecting lines are magenta-colored) and superposition of the abrupt anomalies $C_{LS} \leftrightarrows B_{HS}$ or $C_{LS} \leftrightarrows B_{HS} \leftrightarrows A_{HS}$ (green dots connected by green lines) on the smooth anomalies $B_{LS} \leftrightarrows B_{HS}$ (sets of experimental points and connecting lines are orange-colored).

those given in the last paragraph and are therefore not discussed here in detail.

The discovery of the latter two groups of solvates, whose $\mu_{eff}(T)$ dependences revealed a similar type of structural change at different temperatures (Figure 12a and 12b), allowed us to describe the magnetostructural correlations for breathing crystals with aromatic solvent guest molecules from a single viewpoint. The description is based on two factors. First, the thermally induced structural rearrangement of $Cu(hfac)_2L \cdot 0.5Solv$ crystals that provokes the magnetic anomalies on the $\mu_{eff}(T)$ curve is extremely sensitive to the structure of the solvent guest molecules. Second, the thermally induced structural changes in the heterospin chains themselves strictly correlate with the orientation of solvent molecules in the interchain space; only strictly definite orientations of these molecules are possible, which we designated as A, B, and C. The variation of temperature (especially during the phase transformation) initiates great numbers of coherent motions of atoms in the polymer chains as well as the motions of chains relative to one another and to solvate molecules in the interchain space in crystal. This ensures the integrity and mechanical stability of the single crystal over a wide temperature range and ultimately makes it possible to solve its crystal and molecular structure both before and after the transition.[5−13,29,50]

The temperature-sensitive $Cu(hfac)_2L \cdot 0.5Solv$ crystals additionally contain rather rigid fragments (the benzene ring in the Solv guest molecules and the bond lengths and angles in the nitronyl nitroxide molecule), whose geometrical characteristics do not change at different temperatures. The distances between the butyl-substituted N atom and the nearest C atom in the pyrazole ring of the L ligand range from 1.315(5) to 1.353(8) Å over the whole range of temperatures for the same $Cu(hfac)_2L \cdot 0.5(1\text{-}CH_3\text{-}4\text{-}C_2H_5{-}C_6H_4)$ single crystal and from 1.319(3) to 1.335(2) Å for $Cu(hfac)_2L \cdot 0.5C_4H_9{-}C_6H_5$. The change in the C−C bond lengths between the imidazoline and pyrazole rings of L is 1.422(6)−1.464(9) Å in $Cu(hfac)_2L \cdot 0.5(1\text{-}CH_3\text{-}4\text{-}C_2H_5{-}C_6H_4)$ and 1.435(3)−1.447(2) Å in $Cu(hfac)_2L \cdot 0.5C_4H_9{-}C_6H_5$. The angle between the planes of the $CN_2$ fragment of the imidazoline ring and the pyrazole ring is 2.47−4.77° in $Cu(hfac)_2L \cdot 0.5(1\text{-}CH_3\text{-}4\text{-}C_2H_5{-}C_6H_4)$ and 2.90−3.75° in $Cu(hfac)_2L \cdot 0.5C_4H_9{-}C_6H_5$ at different temperatures, the change being very insignificant for both. The $Cu{-}O_{NO}$ distance, however, changes substantially, from 2.311(3) to 2.044(6) Å in $Cu(hfac)_2L \cdot 0.5(1\text{-}CH_3\text{-}4\text{-}C_2H_5{-}C_6H_4)$ and from 2.325(1) to 2.004(1) Å in $Cu(hfac)_2L \cdot 0.5C_4H_9{-}C_6H_5$. The change in the $Cu{-}O_{NO}$ distance is exactly the factor that modulates the exchange coupling energy in $>N{-}^{\bullet}O{-}Cu^{II}{-}O^{\bullet}{-}N<$ exchange clusters. Summarizing the results, we draw the conclusion that the structural transformations and the ensuing magnetic anomalies under study can be divided into the groups shown in Table 2.

Items 1 and 2 refer to the A-type interchain orientation of the solvent dominating in the structure at high temperatures and 3 and 4 to the B-type. The subscript LS means low spin and HS high spin. If we have the A orientation at low temperatures and it does not change at high temperatures, the fraction of high-spin $>N{-}^{\bullet}O{-}Cu^{II}{-}O^{\bullet}{-}N<$ exchange clusters gradually increases with temperature, and this is reflected on the $\mu_{eff}(T)$ curve as a gradually increasing effective magnetic moment. The transition from the low- to the high-spin state for the clusters lies in the temperature range ∼100−140 K and occurs smoothly (Figure 12a). If, however, the starting interchain orientation of the solvent in the low-temperature phase is the C type and the solvent is such that its molecules can be reorientated to A at elevated temperatures, the magnetic anomalies lies in the temperature range ∼115−135 K (Figure 8), which actually lies in the range of $A_{LS} \leftrightarrows A_{HS}$ transformations (100−140 K). The $C_{LS} \leftrightarrows A_{HS}$ transition is abrupt in this case. Figure 13 demonstrates a superposition of the $C_{LS} \leftrightarrows A_{HS}$ anomalies (blue) with the smooth anomalies corresponding to the $A_{LS} \leftrightarrows A_{HS}$ transformations (magenta).

As in the case of the $A_{LS} \leftrightarrows A_{HS}$ transformation, if we have the B orientation at low temperatures which is retained at high temperatures, the fraction of high-spin $>N{-}^{\bullet}O{-}Cu^{II}{-}O^{\bullet}{-}N<$ exchange clusters gradually increases at elevated temperatures; this is reflected as a gradual increase in the effective magnetic moment on the $\mu_{eff}(T)$ curve. The $B_{LS} \leftrightarrows B_{HS}$ transition, however, is much more hindered than $A_{LS} \leftrightarrows A_{HS}$ and occurs at higher temperatures. The transition is smooth and more expanded in temperature (∼120−300 K in Figure 12b). If, however, the starting interchain orientation of the aromatic solvent in the low-temperature phase is C and the solvent is such that its molecules can change orientation to B (or at first B and then A) at elevated temperatures, the magnetic anomalies lie in the temperature range ∼170−200 K (Figure 8) in the range of the $B_{LS} \leftrightarrows B_{HS}$ transformations. The $C_{LS} \leftrightarrows B_{HS}$ (or $C_{LS} \leftrightarrows B_{HS}$ and then $B_{HS} \leftrightarrows A_{HS}$) transition is abrupt. In Figure 13, this is demonstrated by the superposition of the green-colored $C_{LS} \leftrightarrows B_{HS}$ (or $C_{LS} \leftrightarrows B_{HS}$ and then $B_{HS} \leftrightarrows A_{HS}$) anomalies on the smooth orange-colored $B_{LS} \leftrightarrows B_{HS}$-type anomalies.

In the group of aromatic solvates under study, $Cu(hfac)_2L \cdot 0.5C_6H_6$ and $Cu(hfac)_2L \cdot 0.5CH_3{-}C_6H_5$ show magnetic anomalies at very low temperatures, the effect being one-half as wide as that for all other compounds (Figure 2). For these compounds, $\mu_{eff}$ is ∼2.48 $\beta$ at room temperature and ∼2.15 $\beta$ at $T$ < 30 K for $Cu(hfac)_2L \cdot 0.5C_6H_6$ and $Cu(hfac)_2L \cdot 0.5CH_3{-}C_6H_5$ (Figure 2). It is logical to explain this by the smallest size of the benzene and toluene molecules compared to the sizes of other aromatic solvents in $Cu(hfac)_2L \cdot 0.5Solv$. The crystals should therefore be cooled to very low temperatures for

the magnetic anomaly to show itself in this case. Even then spin coupling, however, does not occur in all >N−•O−Cu$^{II}$−O•−N< exchange clusters. A similar effect was earlier observed for solvates with hexane, amyl chloride, and amyl bromide.[13]

According to XRD data for Cu(hfac)$_2$L·0.5CH$_3$−C$_6$H$_5$, the bond lengths Cu−O$_{NO}$ decrease while Cu−O$_{hfac}$ simultaneously increase in the CuO$_6$ units when the temperature is lowered to 30 K, reflecting the gradual transition of the nitroxyl O atom from axial to equatorial position. Note that at 30 K the structure of the complex for Cu(hfac)$_2$L·0.5CH$_3$−C$_6$H$_5$ is refined with the average Cu−O$_{NO}$ distance 2.089(2) Å, while the characteristic Cu−O$_{NO}$ bond length is generally ∼2.3 and ∼2.0 Å in complexes with axial and equatorial coordination, respectively.[1,2,10,11,13,23,48] Since XRD analysis reflects only the integral picture in the absence of long-range ordering, the >N−•O−Cu$^{II}$−O•−N< exchange clusters, in which the Cu−O$_{NO}$ bond lengths are abruptly shortened, are presumably randomly distributed over the crystal in the low-temperature modification of Cu(hfac)$_2$L·0.5CH$_3$−C$_6$H$_5$. By analogy with the data of refs 10, 11, 13, 16, and 23 we can conclude that a strong antiferromagnetic exchange interaction dominates below 30 K in one-half of all >N−•O−Cu$^{II}$−O•−N< exchange clusters, due to which the effective magnetic moment decreases. The calculated abrupt change should be 0.38 $\beta$ with the assumption that $g_{Cu}$ = 2.18 and $g_L$ = 2.0; this agrees well with the experimental decrease (0.33 $\beta$) in $\mu_{eff}$ for Cu(hfac)$_2$L·0.5CH$_3$−C$_6$H$_5$ (Figure 2). In the CuN$_2$O$_4$ units, the Cu−N distances also decrease at lower temperatures but to a much less significant extent than the Cu−O$_{NO}$ distances. According to the given notation (Table 2), the transition from the low- to the high-temperature phase is a B$_{LS}$ ⇆ B$_{HS}$-type transition (Figures S11 and S12, Supporting Information).

For Cu(hfac)$_2$L·0.5C$_6$H$_6$, an XRD study was carried out at 295, 240, 150, and 100 K (Figures S11b and S12b, Supporting Information). Numerous attempts to study its structure at ∼30 K failed because of crystal decomposition during the phase transition. The $\mu_{eff}(T)$ dependences for Cu(hfac)$_2$L·0.5C$_6$H$_6$ and Cu(hfac)$_2$L·0.5CH$_3$−C$_6$H$_5$ being very similar (Figure 2; they differ only in the transition temperature), we can assume that the structural rearrangement in solid Cu(hfac)$_2$L·0.5C$_6$H$_6$ is similar to the one in Cu(hfac)$_2$L·0.5CH$_3$−C$_6$H$_5$.

## CONCLUSIONS

Our XRD and magnetochemical studies of a series of synthesized Cu(hfac)$_2$L·0.5Solv polymer-chain complexes with aromatic solvent guest molecules showed that the observed magnetic anomalies allow changes in the spin state of >N−•O−Cu$^{II}$−O•−N< exchange clusters during the thermally induced structural rearrangement of Jahn−Teller coordination units. The resulting form of the magnetic anomaly on the $\mu_{eff}(T)$ curve and the temperature of the effect depends on the type of the orientation of solvate molecules in crystal and the change in this orientation during the structural transformation. The analysis of magnetostructural correlations inherent in Cu(hfac)$_2$L·0.5Solv revealed the main types of transformation: A$_{LS}$ ⇆ A$_{HS}$ or C$_{LS}$ ⇆ A$_{HS}$ and B$_{LS}$ ⇆ B$_{HS}$ or C$_{LS}$ ⇆ B$_{HS}$ (or C$_{LS}$ ⇆ B$_{HS}$ ⇆ A$_{HS}$). These types of transitions determine the form of the magnetic anomaly on the $\mu_{eff}(T)$ curve, namely, its temperature range and abruptness. The $\mu_{eff}(T)$ dependence for Cu(hfac)$_2$L·0.5Solv solvates being discussed can thus serve as an indicator of their supramolecular organization, namely, the existence of definite voids between chains and a definite position of the aromatic solvent molecule in these voids. The volume of the void with the solvent and the crystal density change smoothly in the course of the A$_{LS}$ ⇆ A$_{HS}$ and B$_{LS}$ ⇆ B$_{HS}$ transformations but abruptly and unpredictably during the C$_{LS}$ ⇆ A$_{HS}$ and C$_{LS}$ ⇆ B$_{HS}$ (or C$_{LS}$ ⇆ B$_{HS}$ ⇆ A$_{HS}$) transitions (Table 1).

When there is no possibility for reorientations of interchain solvate molecules (A$_{LS}$ ⇆ A$_{HS}$ and B$_{LS}$ ⇆ B$_{HS}$ transformations) in the crystal at elevated temperatures, the number of >N−•O−Cu$^{II}$−O•−N< exchange clusters with long Cu−O$_{NO}$ distances with dominant ferromagnetic exchange gradually increases. The anomalies on the $\mu_{eff}(T)$ curves are then smoother, and the transition region between the low- and the high-temperature phases lies in a wide temperature range; the gradual increase in the effective magnetic moment corresponds to the gradual increase in the average Cu−O$_{NO}$ bond length obtained by XRD. If, however, the solvate is in the low-spin C$_{LS}$ state at low temperatures, a reorientation of the interchain solvate molecules is possible on heating (C$_{LS}$ ⇆ A$_{HS}$, C$_{LS}$ ⇆ B$_{HS}$, or C$_{LS}$ ⇆ B$_{HS}$ ⇆ A$_{HS}$ transformations). In this case, the structural transformation occurs abruptly. The transition to the high-temperature value of $\mu_{eff}$ is also abrupt. If the transition occurs from the C to the A phase, the temperature of the maximum of the derivative $\partial\mu_{eff}/\partial T$ is approximately 70−100 degrees lower than during the transition from C to B (Figure 13).

Thus, our study of Cu(hfac)$_2$L·0.5Solv polymer chain heterospin solvates showed that there is a clear relationship between the temperature-induced reorientation of aromatic solvate molecules in the interchain space of crystals and the form of the magnetic anomaly; the anomaly can be described by the corresponding type of transformation from low- to high-spin phase: A$_{LS}$ ⇆ A$_{HS}$, C$_{LS}$ ⇆ A$_{HS}$, B$_{LS}$ ⇆ B$_{HS}$, C$_{LS}$ ⇆ B$_{HS}$ ⇆ A$_{HS}$, or C$_{LS}$ ⇆ B$_{HS}$.

## ASSOCIATED CONTENT

**Supporting Information.** Structural determination parameters, crystal, and structure refinement data, atomic coordinates, and isotropic displacement parameters for all complexes (in CIF form; Figures S1−S12). This material is available free of charge via the Internet at http://pubs.acs.org.

## AUTHOR INFORMATION

**Corresponding Author**

*E-mail: Victor.Ovcharenko@tomo.nsc.ru.

## ACKNOWLEDGMENT

This work was supported by RFBR (grant nos. 09-03-00091, 09-03-12108, and 11-03-00027), State contract P2439, RAS, and SB RAS.

## REFERENCES

(1) Lanfranc de Panthou, F.; Belorizky, E.; Calemczuk, R.; Luneau, D.; Marcenat, C.; Ressouche, E.; Turek, P.; Rey, P. *J. Am. Chem. Soc.* **1995**, *117*, 11247–11253.

(2) Lanfranc de Panthou, F.; Luneau, D.; Musin, R.; Öhrström, L.; Grand, A.; Turek, P.; Rey, P. *Inorg. Chem.* **1996**, *35*, 3484–3491.

(3) Iwahory, F.; Inoue, K.; Iwamura, H. *Mol. Cryst. Liq. Cryst.* **1999**, *334*, 533–538.

(4) Caneschi, A.; Chiesi, P.; David, L.; Ferraro, F.; Gatteschi, D.; Sessoli, R. *Inorg. Chem.* **1993**, *32*, 1445–1453.

(5) Baskett, M.; Lahti, P. M.; Paduan-Filho, A.; Oliveira, N. F., Jr. *Inorg. Chem.* **2005**, *44*, 6725–6735.
(6) Okazawa, A.; Hashizume, D.; Ishida, T. *J. Am. Chem. Soc.* **2010**, *132*, 11516–11524.
(7) Ovcharenko, V. I.; Fokin, S. V.; Romanenko, G. V.; Shvedenkov, Yu. G.; Ikorskii, V. N.; Tretyakov, E. V.; Vasilevsky, S. F. *Russ. J. Struct. Chem. (Engl. Transl.)* **2002**, *43*, 153–169.
(8) Ovcharenko, V. I.; Fokin, S. V.; Romanenko, G. V.; Ikorskii, V. N.; Tretyakov, E. V.; Vasilevsky, S. F.; Sagdeev, R. Z. *Mol. Phys.* **2002**, *100*, 1107–1115.
(9) Rey, P.; Ovcharenko, V. I. In *Magnetism: Molecules to Materials, IV*; Miller, J. S., Drillon, M., Eds.; Wiley-VCH: New York, 2003; pp 41−63.
(10) Ovcharenko, V. I.; Maryunina, K. Yu.; Fokin, S. V.; Tretyakov, E. V.; Romanenko, G. V.; Ikorskii, V. N. *Russ. Chem. Bull. (Engl. Transl.)* **2004**, *11*, 2406–2427.
(11) Fokin, S.; Ovcharenko, V.; Romanenko, G.; Ikorskii, V. *Inorg. Chem.* **2004**, *43*, 969–977.
(12) Maryunina, K.; Fokin, S.; Ovcharenko, V.; Romanenko, G.; Ikorskii, V. *Polyhedron* **2005**, *24*, 2094–2101.
(13) Ovcharenko, V. I.; Romanenko, G. V.; Maryunina, K. Yu.; Bogomyakov, A. S.; Gorelik, E. V. *Inorg. Chem.* **2008**, *47*, 9537–9552.
(14) Fedin, M.; Veber, S.; Gromov, I.; Ovcharenko, V.; Sagdeev, R.; Schweiger, A.; Bagryanskaya, E. *J. Phys. Chem. A* **2006**, *110*, 2315–2317.
(15) Fedin, M.; Veber, S.; Gromov, I.; Ovcharenko, V.; Sagdeev, R.; Bagryanskaya, E. *J. Phys. Chem. A* **2007**, *111*, 4449–4455.
(16) Fedin, M.; Veber, S.; Gromov, I.; Maryunina, K.; Fokin, S.; Romanenko, G.; Sagdeev, R.; Ovcharenko, V.; Bagryanskaya, E. *Inorg. Chem.* **2007**, *46*, 11405–11415.
(17) Veber, S. L.; Fedin, M. V.; Potapov, A. I.; Maryunina, K. Yu.; Romanenko, G. V.; Sagdeev, R. Z.; Ovcharenko, V. I.; Goldfarb, D.; Bagryanskaya, E. G. *J. Am. Chem. Soc.* **2008**, *130*, 2444–2445.
(18) Veber, S. L.; Fedin, M. V.; Romanenko, G. V.; Sagdeev, R. Z.; Bagryanskaya, E. G.; Ovcharenko, V. I. *Inorg. Chim. Acta* **2008**, *361*, 4148–4152.
(19) Fedin, M.; Ovcharenko, V.; Bagryanskaya, E. In *The Treasures of Eureka, I: Electron Paramagnetic Resonance: From Fundamental Research to Pioneering Applications and Zavoisky Award*; Salikhov, K. M., Ed.; AXAS Publishing Ltd.: Wellington, New Zealand, 2009; pp 122−123.
(20) Fedin, M. V.; Veber, S. L.; Sagdeev, R. Z.; Ovcharenko, V. I.; Bagryanskaya, E. G. *Russ. Chem. Bull. (Engl. Transl.)* **2010**, *59*, 1065–1079.
(21) Fedin, M.; Ovcharenko, V.; Sagdeev, R.; Reijerse, E.; Lubitz, W.; Bagryanskaya, E. *Angew. Chem., Int. Ed.* **2009**, *47*, 6897–6899.
(22) Osip'yan, Yu. A.; Morgunov, R. B.; Baskakov, A. A.; Ovcharenko, V. I.; Fokin, S. V. *Phys. Solid State* **2003**, *45*, 1465–1470.
(23) Zueva, E. M.; Ryabykh, E. R.; Kuznetsov, An. M. *Russ. Chem. Bull. (Engl. Transl.)* **2009**, *8*, 1654–1662.
(24) Postnikov, A. V.; Galakhov, A. V.; Blügel, S. *Phase Transitions* **2005**, *78*, 689–699.
(25) Vancoillie, S.; Rulíšek, L.; Neese, F.; Pierloot, K. *J. Phys. Chem. A* **2009**, *113*, 6149–6157.
(26) Morozov, V. A.; Lukzen, N. N.; Ovcharenko, V. I. *J. Phys. Chem. B* **2008**, *112*, 1890–1893.
(27) Morozov, V. A.; Lukzen, N. N.; Ovcharenko, V. I. *Russ. Chem. Bull. (Engl. Transl.)* **2008**, *4*, 863–867.
(28) Morozov, V. A.; Lukzen, N. N.; Ovcharenko, V. I. *Dokl. Phys. Chem.* **2010**, *430* (Part 2), 33–35.
(29) Ovcharenko, V. I. In *Stable Radicals: Fundamentals and Applied Aspects of Odd-Electron Compounds*; Hicks, R., Ed.; Wiley-VCH: New York, 2010; pp 461−506.
(30) Sorai, M.; Ensling, J.; Hasselbach, K. M.; Gütlich, P. *Chem. Phys.* **1977**, *20*, 197–208.
(31) Gütlich, P.; Köppen, H.; Steinhäuser, H. G. *Chem. Phys. Lett.* **1980**, *74*, 475–480.
(32) Gütlich, P.; Hauser, A.; Spiering, H. *Angew. Chem., Int. Ed.* **1994**, *33*, 2024–2054.
(33) Murray, K. S.; Kepert, C. J. In *Topics in Current Chemistry*; Gütlich, P., Goodwin, H. A., Eds.; Springer-Verlag: Berlin, Heidelberg, 2004; Vol. 233, pp 216−219.
(34) Sorai, M. In *Topics in Current Chemistry*; Gütlich, P., Goodwin, H. A., Eds.; Springer-Verlag: Berlin, Heidelberg, 2004; Vol. 235, pp 151−161.
(35) Katz, B. A.; Strouse, C. E. *J. Am. Chem. Soc.* **1979**, *101*, 6214–6221.
(36) Mikami, M.; Konno, M.; Saito, Y. *Chem. Phys. Lett.* **1979**, *63*, 566–569.
(37) Greenaway, A. M.; Sinn, E. *J. Am. Chem. Soc.* **1978**, *100*, 8080–8084.
(38) Greenaway, A. M.; O'Connor, C. J.; Schrock, A.; Sinn, E. *Inorg. Chem.* **1979**, *18*, 2692–2695.
(39) Wiehl, L.; Kiel, G.; Köhler, C. P.; Spiering, H.; Gütlich, P. *Inorg. Chem.* **1986**, *25*, 1565–1571.
(40) Cecconi, F.; Di Vaira, M.; Midollini, S.; Orlandini, A.; Sacconi, L. *Inorg. Chem.* **1981**, *20*, 3423–3430.
(41) Hostettler, M.; Törnroos, K. W.; Chernyshov, D.; Vangdal, B.; Bürgi, H.-B. *Angew. Chem., Int. Ed.* **2004**, *43*, 4589–4594.
(42) Halder, G. J.; Kepert, C. J.; Moubaraki, B.; Murray, K. S.; Cashion, J. D. *Science* **2002**, *298*, 1762–1765.
(43) Törnroos, K. W.; Hostettler, M.; Chernyshov, D.; Vangdal, B.; Bürgi, H.-B. *Chem.—Eur. J.* **2006**, *12*, 6207–6215.
(44) Neville, S. M.; Halder, G. J.; Chapman, K. W.; Duriska, M. B.; Southon, P. D.; Cashion, J. D.; Létard, J.-F.; Moubaraki, B.; Murray, K. S.; Kepert, C. J. *J. Am. Chem. Soc.* **2008**, *130*, 2869–2876.
(45) Dîrtu, M. M.; Rotaru, A.; Gillard, D.; Linares, J.; Codjovi, E.; Tinant, B.; Garcia, Y. *Inorg. Chem.* **2009**, *48*, 7838–7852.
(46) Fedin, M. V.; Veber, S. L.; Maryunina, K. Yu.; Romanenko, G. V.; Suturina, E. A.; Gritsan, N. P.; Sagdeev, R. Z.; Ovcharenko, V. I.; Bagryanskaya, E. G. *J. Am. Chem. Soc.* **2010**, *132*, 13886–13891.
(47) Ovcharenko, V.; Fursova, E.; Romanenko, G.; Eremenko, I.; Tretyakov, E.; Ikorskii, V. *Inorg. Chem.* **2006**, *45*, 5338–5350.
(48) Musin, R. N.; Schastnev, P. V.; Malinovskaya, S. A. *Inorg. Chem.* **1992**, *31*, 4118–4121.
(49) Hayami, S.; Shigeyoshi, Y.; Akita, M.; Inoue, K.; Kato, K.; Osaka, K; Takata, M.; Kawajiri, R.; Mitani, T.; Maeda, Y. *Angew. Chem., Int. Ed.* **2005**, *44*, 4899–4903.
(50) Okazawa, A.; Ishida, T. *Inorg. Chem.* **2010**, *49*, 10144–10147.